ISSN 2822-2881

Firat University Journal of Experimental and Computational Engineering

Volume: 2 Issues: 3 Year: 2023

www.fujece.firat.edu.tr

Firat University Journal of Experimental and Computational Engineering

Fırat Üniversitesi Deneysel ve Hesaplamalı Mühendislik Dergisi

Volume: 2 Issues: 3 Year: 2023

Firat University Journal of Experimental and Computational Engineering

Fırat Üniversitesi Deneysel ve Hesaplamalı Mühendislik Dergisi

Volume: 2 Issues: 3 Year: 2023

Correspondence Address

Firat University Faculty of Engineering Journal of Experimental and Computational Engineering Publishing Coordinatorship
23119 Elazığ/TÜRKİYE

E-mail: fujece@firat.edu.tr
Web page: http://fujece.firat.edu.tr/

Firat University Journal of Experimental and Computational Engineering a peer-reviewed journal.

Firat University Journal of Experimental and Computational Engineering

Fırat Üniversitesi Deneysel ve Hesaplamalı Mühendislik Dergisi

Volume: 2 Issues: 3 Year: 2023

CONTENTS

Firat Univ Jour. of Exp. and Comp. Eng., 2(3), 97-103, 2023

Firat University Journal of Experimental and Computational Engineering
Fırat Üniversitesi Deneysel ve Hesaplamalı Mühendislik Dergisi

Comparison of Photoelectric Conversion Efficiencies of DSSCs Sensitized with Velvet Red Rose and Ivy Rose Dye

Kadife Kırmızı Gül ve Sarmaşık Gül Boyası ile Duyarlılaştırılan Boya Duyarlı Güneş Pillerinin Fotoelektrik Dönüşüm Verimlerinin Karşılaştırılması

Fehmi ASLAN[1]*

[1]Department of Motor Vehicles and Transportation Technologies, Yesilyurt Vocational School, Malatya Turgut Ozal University, Malatya, 44210, Turkey.

[1]fehmi.aslan@ozal.edu.tr

Received: 28.08.2023
Accepted: 16.10.2023
Revision: 29.09.2023
doi: 10.5505/fujece.2023.03522
Research Article

Citation: Aslan F. "Comparison of photoelectric conversion efficiencies of dsscs sensitized with velvet red rose and ivy rose dye". *Firat University Journal of Experimental and Computational Engineering*, 2(3), 97-103, 2023.

Abstract
In this study, extracts from velvet red rose and ivy rose were used as sensitizers in dye-sensitized solar cells. XRD analyses confirmed the anatase structure of the TiO_2 thin film. SEM photographs showed that the nanospheres were in tight contact with each other, allowing for greater dye absorption on the TiO_2 surface. It was understood from the UV-vis analysis that the velvet red rose dye exhibited a wider absorption in the visible region. The I-V characterizations showed that cell sensitized with velvet red rose dye exhibited higher cell performance (η=0.12) than DSSC sensitized with ivy rose dye.

Keywords: Dye-sensitive solar cells, Natural dyes, Photovoltaic performance

Özet
Bu çalışmada, kadife kırmızı gül ve sarmaşık gül bitkisinden elde edilen özütler, boya duyarlı güneş pillerinde duyarlılaştırıcı olarak kullanıldı. XRD analizleri, TiO_2 ince filmin anataz yapısını doğruladı. SEM fotoğrafları, nanokürelerin birbirleriyle sıkı temas halinde olduğunu ve TiO_2 yüzeyinde daha fazla boya emilimine izin verdiğini gösterdi. UV-vis analizinden, kadife kırmızı gül boyasının görünür bölgede daha geniş bir absorpsiyon sergilediği anlaşıldı. I-V karakterizasyonları incelendiğinde kadife kırmızı gül boyası ile duyarlı hale getirilen hücrenin sarmaşık gül boyası ile duyarlı hale getirilen hücre'ye göre daha yüksek hücre performansına (η=0.12)sahip olduğu görüldü.

Anahtar kelimeler: Boya duyarlı güneş pilleri, Doğal boyalar, Fotovoltaik performans

1. Introduction

Photovoltaic technology is attractive because it converts light energy directly into electrical energy [1]. The high cost and non-reversible nature of silicon-based solar cells have made it inevitable for new technologies to emerge in this field [2]. In this field, dye-sensitized solar cells (DSSCs)are very attractive due to their ease of manufacture and low cost [3]. A typical DSSC; consists of a photoanode layer, counter electrode, sensitizing dye, redox electrolyte, and counter electrode [4].

Sensitizing dyes produced from some natural plants exhibit remarkable absorption in the visible region. This feature positively affects the performance of DSSCs [5]. The highest cell yields for DSSCs were achieved with Ru-based dyes [6]. However, these dyes' high costs and toxic properties have accelerated the studies on alternative sensitizers [7]. In this context, dyes extracted from natural plants are promising for DSSCs. Natural dyes containing some flavonoid groups provided high power conversion efficiency in DSSCs [8]. Although many rose species have been used as sensitizers in DSSCs, no study using velvet red rose and ivy rose species has been reported before. In a study reported by Roy et al.,

*Corresponding author

Plagiarism Checks: Yes – Turnitin
Complaints: fujece@firat.edu.tr

efficiency values of up to 2.09 % were achieved in DSSCs sensitized with *Rose bengal* dye [9]. In another study by Siregar et al., Mg-modified photoanodes achieved efficiency values as high as 3.53 % in DSSCs sensitized with *Rose myrtle* [10]. In a different study reported by Waghmare et al., TiO_2-ZrO_2 based photoelectrodes were sensitized with *Rose bengal* and the highest cell performance was recorded as 0.038 % [11]. In this study, it was investigated how sensitizers extracted from velvet red rose and ivy rose affected the performance of DSSCs. Photographs of the flowers from which the dyes were extracted can be seen in Figure 1.

Figure 1. a) Red velvet rose b) Ivy rose

2. Research Significance

In this study, the effect of dyes extracted from velvet red rose plants and ivy rose plants on DSSCs was investigated. The aim of this study is how sensitizers produced from different species of two plants of the same genus affect power conversion efficiency. In this context, two different rose species were extracted using the Soxhlet method. It was determined that there were significant changes in the photovoltaic parameters of DSSCs produced using two different sensitizers. This is because the sensitizing sizes have different phenolic contents. In particular, dyes with high anthocyanin content show better cell performance in DSSCs. The highlights of this study are given below.

Highlights:
• DSSC sensitized with velvet red rose dye showed superior cell performance.
• Velvet red rose dye exhibited a wider range of absorption in the visible region.
• The open circuit voltage (Voc=0.5V) of the cell sensitized with the velvet red rose dye is higher than that of the cell sensitized with the ivy rose dye (Voc=0.3V).

3. Experimental Method-Process

3.1. Materials

All materials were used in the experiments without the need for extra purification. In experiments; Titanium IV isopropoxide (TTIP, ≥97.0%, Sigma-Aldrich), ethyl alcohol (≥99.5%, Sigma-Aldrich), urea (Chemsolid), terpineol (Sigma-Aldrich), ethyl cellulose (Sigma-Aldrich), FTO (Florine doped tin oxide) conductive glass (RS < 15 Ω/Sq Sigma), counter electrode (Platinum: Solaronix), redox electrolyte solution (Solaronix) used.

3.2. Production of TiO_2 nanoparticles

In this study, the sol-gel method was used for the production of TiO_2 nanoparticles. 6 ml of TTIP was dissolved in 5 ml of isopropanol. 75 ml of distilled water and 2.5 ml of citric acid were added to this mixture and vigorously stirred at 80 °C for 4 h. After 4 h, the viscous solution formed was centrifuged and the precipitate formed was washed several times with pure and then sintered at 450 °C for 2 h. The white particles formed were crushed in an agate mortar and turned into powder.

3.3. Extraction of plant dyes

Velvet red rose and ivy rose leaves were washed several times with distilled water and dried in a vacuum oven in the dark for one day. The dried leaves were pulverized in a high-speed grinder. 5 g of each dye extract was taken and placed in soxhlet cartridges containing 100 ml of alcohol separately. It was waited until the systems siphoned 5 times, then waited for it to cool down. The cooled extracted dyes were stored in a dark environment at 4 °C until used in the experiments. The beaten rose leaves and the soxhlet system is shown in Fig. 2.

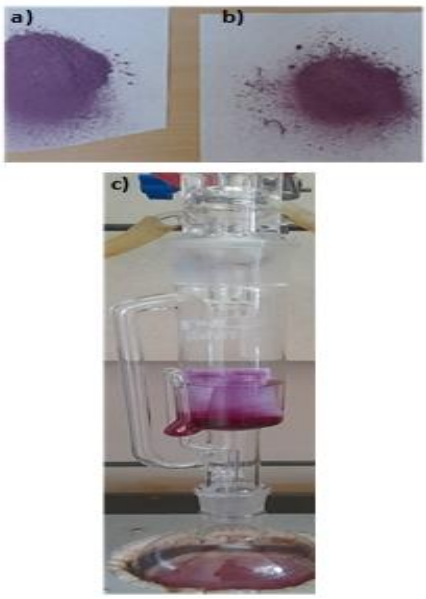

Figure 2. a) Ivy rose extract, b) Velvet red rose extract, c) Production of dyes with the Soxhlet system

3.4. Production of DSSCs

For TiO_2 paste making, 1.5 g TiO_2, some ethyl cellulose, and a few drops of terpineol were mixed in an agate mortar to obtain the appropriate paste consistency. TiO_2 paste was coated with the doctor blade method [12] on the conductive surface of the FTO glasses, which were previously cleaned with alcohol and pure water. It was sintered at 450 °C for 45 min to form the photoanode layer. Photoanodes taken from the muffle furnace were immersed in the dye for 24 h after cooling. A few drops of electrolyte solution were dropped on the dye-sensitized photoanodes and closed with a Pt counter electrode. Then the measurement process was started. The photoanodes produced are given in Fig. 3.

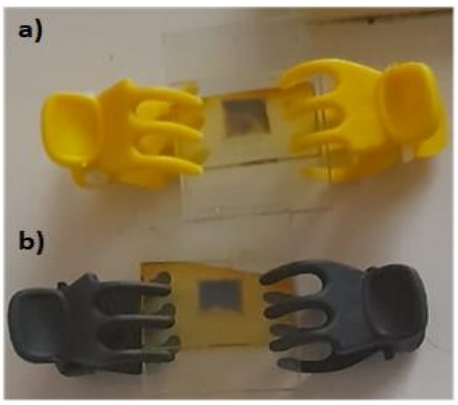

Figure 3. DSSCs a) sensitized with ivy rose dye, b) sensitized with velvet red rose dye

3.5. Characterization

X-ray diffraction (XRD) analyses were performed with Rigaku ManiFlex-600, Scanning electron microscope (SEM) images with Zeiss sigma 300, and UV measurements with UV-3600-Shimadzu-Japan. Electrochemical impedance spectroscopy (EIS) measurements were taken with the Fytronix Impedance Analysis System and I-V measurements were taken with the Fytronix Solar Simulator LSS 9000 I-V Characterization System.

4. Findings and Discussions

The structural analysis of TiO_2 particles produced by the sol-gel method is shown in Fig. 4. The crystal planes corresponding to the 2θ angles in the given Fig. 4 show that TiO_2 is in anatase structure [13]. For high-performance DSSCs, the anatase phase of TiO_2 is very important.

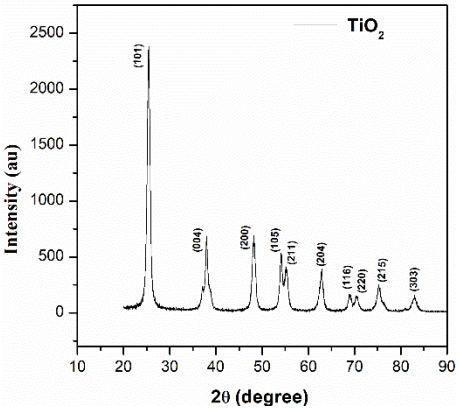

Figure 4. XRD diffraction pattern of produced TiO_2

SEM images in Fig. 5 show the presence of spherical particles. The tight contact between these particles improves electron transport on the photoanode surface [14]. In addition, the presence of tightly packed nanospheres allows better dye absorption on the surface. On the other hand, the presence of such a morphological feature may facilitate charge transport at the interface.

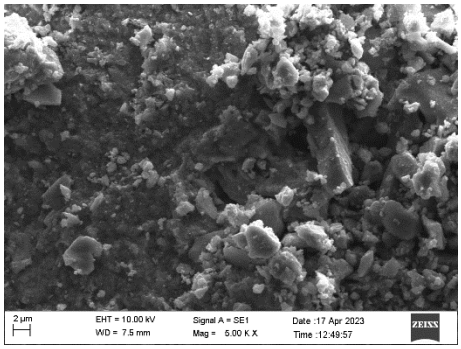

Figure 5. SEM image of TiO_2 particles.

Fig. 6 reflects the UV analysis of natural dyes extracted from two different rose varieties. The dyes obtained from both rose varieties exhibited absorption in a wide wavelength range at 300-700 nm. The dye of the velvet red rose has an extra absorption peak in the wavelength range of 500-600 nm. This absorption behavior can be explained by the higher cell performance of the velvet red rose (η=0.12).

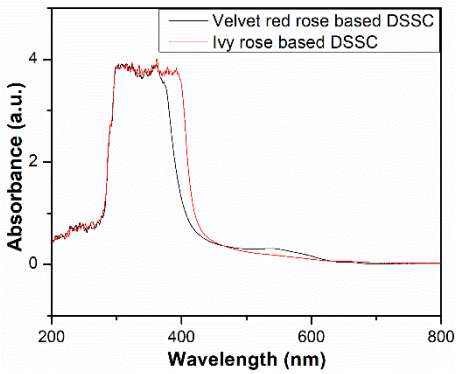

Figure 6. Absorption curves of extracted dyes

The photovoltaic parameters of the produced DSSCs are given in Fig. 7 and summarized in Table 1. When Table 1 was examined, it was seen that the cell sensitized with velvet red rose dye had higher power conversion efficiency than the cell sensitized with ivy rose dye. This can be explained by the high interaction of carbonyl and hydroxyl groups with the TiO_2 surface and stronger absorption in the visible region in the velvet red rose dye [15].

Table 1. Photovoltaic parameters of the produced cells

Sample	J_{sc} (mA/cm^2)	V_{oc} (V)	FF	η (%)
Velvet red rose-based DSSC	0.55	0.5	0.46	0.12
Ivy rose-based DSSC	0.70	0.3	0.35	0.07

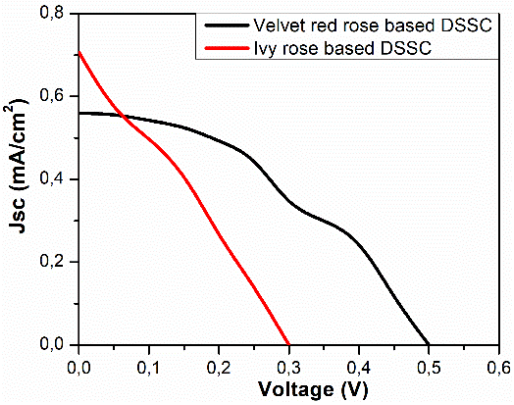

Figure 7. I-V curves of produced DSSCs

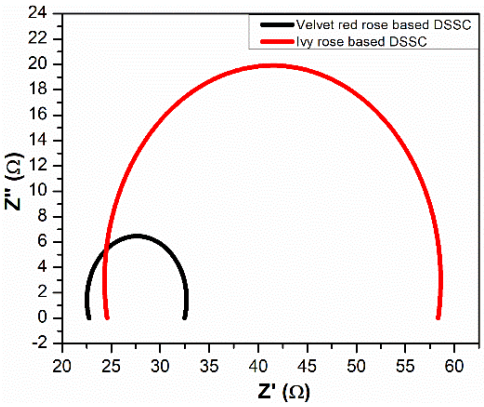

Figure 8. Nyquist curves of DSSCs sensitized with different dyes

EIS analyzes are used to comment on the resistance parameters of a DSSC. Thanks to this analysis, comments can be made about cell performance and resistance parameters. The Nyquist curves in Fig. 8 show two semicircles. As the diameter of the semicircles increases, the impedance value of the DSSC increases and the cell efficiencies decrease [16]. The cell sensitized with ivy rose dye has a larger impedance value because it has a larger semicircular diameter. This could be explained by the lower cell performance of the cell sensitized with the ivy rose dye.

5. Conclusion and Recommendations

XRD analyses confirmed the crystal structure of anatase TiO_2. SEM images showed tight contact between the spherical particles, which facilitated electron transfer. UV analyses showed that dyes sensitized with velvet red rose dye exhibited stronger absorption in the visible region. This was explained by the high cell performance of DSSC sensitized with velvet red rose dye. I-V measurements showed that DSSc sensitized with velvet red rose dye exhibited higher power conversion efficiency. This was attributed to the high interaction of the carbonyl and hydroxyl groups found in the red velvet rose dye with the TiO_2 surface. EIS analyses showed that the cell sensitized with ivy rose dye had a greater impedance value. This was explained by the poor cell performance of DSSC sensitized with ivy rose dye.

6. Credit Authorship Contribution Statement

Fehmi Aslan: Conceptualization, Data curation, Formal analysis, Investigation, Methodology, Validation, Visualization, Writing – original draft, Writing - review & editing.

7. Ethics Committee Approval and Conflict of Interest

The authors declare that they have no known competing financial interests or personal relationships that could have appeared to influence the work reported in this paper.

8. References

[1] Kumar BA, Vetrivelan V, Ramalingam G, Manikandan A, Viswanathan S, Boomi P, Ravi G. "Computational studies and experimental fabrication of DSSC device assembly on 2D-layered TiO_2 and MoS2@TiO_2 nanomaterials". *Physica B: Condensed Matter*, 633, 413770, 2022.

[2] Nnorom OO, Onuegbu GC, Etus C. "Photo-performance characteristics of Baphia nitida and rosella dye-sensitized solar cell". *Results in Optics*, 9, 100311, 2022.

[3] Zatirostami A. "A dramatic improvement in the efficiency of TiO_2-based DSSCs by simultaneous incorporation of Cu and Se into its lattice". *Optical Materials*, 117, 111110, 2021.

[4] Peiris D, Ekanayake P, Karunaratne BA, Petra MI. "Improved Performance of DSSC Photoanodes After the Modification of TiO_2 with Reduced Graphene Oxide". *Journal of Electronic Materials*, 50, 1044–1053, 2021.

[5] Singh S, Maurya IC, Sharma S, Kushwaha S, Srivastava P, Bahadur L. "Application of new natural dyes extracted from Nasturtium flowers (Tropaeolum majus) as a photosensitizer in dye-sensitized solar cells". *Optik*, 243 167331, 2021.

[6] Yoo K, Kim JY, Lee JA, Kim JS, Lee DK, Kim K, Kim JY, Kim B, et al. "Completely transparent conducting oxide-free and flexible dye-sensitized solar cells fabricated on plastic substrates". *ACS Nano*, 9, 3760-3771, 2015.

[7] Lee CP, Li CT, Ho KC. "Use of organic materials in dye-sensitized solar cells". *Materials Today*, 20, 267-283, 2017.

[8] Gao F, Wang Y, Shi D, Zhang J, Wang M, Jing X, Humphry BR, Wang P, et al. "Enhance the optical absorptivity of nanocrystalline TiO_2 film with high molar extinction coefficient ruthenium sensitizers for high performance dye-sensitized solar cells". *Journal of the American Chemical Society*, 130, 10720-10728, 2008.

[9] Roy MS, Balraju P, Kumar M, Sharma GD. "Dye-sensitized solar cell based on Rose Bengal dye and nanocrystalline TiO_2". *Solar Energy Materials*, 92, 909-913, 2008.

[10] Siregar N, Panggabean JH, Sirait M, Rajagukguk J, Gultom NS, Sabir FK. "Fabrication of dye-sensitized solar cells (DSSCs) using Mg-doped ZnO as photoanode and extract Rose Myrtle (Rhodomyrtus tomentosa) as natural dye". *International Journal of Photoenergy-Hindawi*, 1, 1-7, 2021.

[11] Waghmare MA, Beedri NI, Ubale AU, Pathan HM. "Fabrication and characterization of Rose Bengal sensitized binary TiO_2-ZrO_2 oxides photo-electrode based dye-sensitized solar cells" *Engineered Science*, 6, 36-43, 2019.

[12] Aslan F. "Increasing the photoelectric convercion efficiency of dye-sensitized solar cells by doping $SrAl_2O_4$:Eu^{+2},Dy^{+3} to TiO_2-based photoanodes". *Physica B: Condensed Matter*, 668, 1-12, 2023.

[13] Sethy PP, Pani TK, Rout S. "Structural and magnetic properties of Ni/C core–shell nanofibers prepared by one step co-axial electrospinning method". *Journal of Materials Science: Materials in Electronics*, 807, 1-15, 2023.

[14] Nelson J, Chandler RE. "Random walk models of charge transfer and transport in dye-sensitized systems". *Coordination Chemistry Reviews*, 248, 1181-1194, 2004.

[15] Calogero G, Marco G, Caramori S, Cazzanti S, Argazzi R, Bignozzi CA. "Natural dye sensitizers for photoelectrochemical cells". *Energy and Environmental Science*, 2, 1162-1172, 2009.

[16] Qi K, Liu S, Chen Y, Xia B, Li GD. "A simple post-treatment with urea solution to enhance the photoelectric conversion efficiency for TiO_2 dye-sensitized solar cells". *Solar Energy Materials and Solar Cells*, 183, 193-199, 2018.

Firat Univ Jour. of Exp. and Comp. Eng., 2(3), 104-116, 2023

Firat University Journal of Experimental and Computational Engineering
Fırat Üniversitesi Deneysel ve Hesaplamalı Mühendislik Dergisi

Enhancing Sustainability in Asphalt Concrete: Utilizing Ceramic Cake Waste and Performance Analysis

Asfalt Betonunda Sürdürülebilirliğin Artırılması: Seramik Kek Atığının Kullanımı ve Performans Analizi

Murat KARACASU[1], Zahir WAFAIE[2], Kadir Berkhan AKALIN[3]*

[1,2]Civil Engineering Department, Engineering and Architectural Faculty, Eskisehir Osmangazi University, Eskisehir, TURKEY
[3]Civil and Environmental Engineering Department, The Pennsylvania State University, State College, PA, USA
[1]muratk@ogu.edu.tr, [2]zahirwafaye2018@gmail.com, [3]kba5465@psu.edu

Received: 01.09.2023
Accepted: 18.10.2023
Revision: 04.10.2023
doi: 10.5505/fujece.2023.24008
Research Article

Citation: Karacasu M, Wafaie Z, Akalın KB. "Enhancing sustainability in asphalt concrete utilizing ceramic cake waste and performance analysis". *Firat University Journal of Experimental and Computational Engineering*, 2(3), 104-116, 2023.

Abstract

The rapid growth of the global population has led to an increased demand for vehicles and industrial products, resulting in heightened production levels. Unfortunately, this surge in production inevitably generates significant amounts of waste, which, when not effectively managed, contributes to environmental pollution and poses challenges for waste storage. To address these pressing concerns, scientific research has been actively exploring ways to repurpose waste materials across various sectors to promote sustainability. This study delves into the innovative concept of incorporating ceramic cake waste (CCW) as an alternative aggregate material in the production of asphalt concrete -a key material in road construction. Our research explored the feasibility of incorporating CCW into asphalt concrete, typically consisting of aggregates and bitumen. We identified a pivotal threshold through rigorous testing and analysis: incorporating up to 20% CCW in asphalt concrete production aligns with industry standards. This approach not only aids in reducing environmental and visual pollution but also optimizes waste storage and resource utilization, ultimately contributing to a healthier environment and improved quality of life. In conclusion, our study takes a significant step towards promoting sustainability in the road construction sector. The findings provide a foundation for the further exploration and adoption of ceramic cake waste reuse in road construction, offering a promising solution and awareness to address the challenges posed by increasing waste generation and the imperative for sustainable development.

Keywords: Asphalt concrete, Ceramic cake, Waste recycling, Marshall design, Sustainable materials

Özet

Küresel nüfusun hızlı büyümesi, araçlara ve endüstriyel ürünlere olan talebin artmasına ve bunun sonucunda üretim seviyelerinin artmasına neden olmaktadır. Ne yazık ki, üretimdeki bu artış kaçınılmaz olarak önemli miktarda atık üretmektedir. Bu atıklar etkili bir şekilde yönetilmediğinde çevre kirliliğine sebep olmakta ve atık depolama konusunda zorluklara yol açmaktadır. Bu sorunları gidermek için sürdürülebilirliği teşvik etmek amacıyla çeşitli sektörlerde atık malzemeleri yeniden kullanmanın yolları bilimsel çalışmalarda aktif olarak araştırılmaktadır. Bu çalışmada, yol yapımında önemli bir malzeme olan asfalt betonu üretiminde seramik kek atığının (SKA) alternatif bir agrega malzemesi olarak kullanılmasına yönelik yenilikçi konsept incelenmektedir. Araştırmamız, SKA'nın, tipik olarak agrega ve bitümden oluşan asfalt betonuna dahil edilmesinin fizibilitesini sunmaktadır. Titiz test ve analizler sonucunda, asfalt betonu üretimine %20'ye kadar SKA'nın dahil edilmesi endüstri standartlarına uygun olduğu belirlenmiştir. Bu yaklaşım çevre ve görsel kirliliğin azaltılmasına yardımcı olurken, aynı zamanda atıkların depolanması ve uygun kullanılması ile daha sağlıklı bir çevreye ve yaşam kalitesinin iyileştirilmesine katkıda bulunmaktadır. Sonuç olarak, çalışmamız yol inşaatı sektöründe sürdürülebilirliğin teşvik edilmesi yönünde önemli bir adım atmaktadır. Bulgular, seramik kek atıklarının yol yapımında yeniden kullanılmasının daha fazla araştırılması ve benimsenmesi için temel oluşturmakta ve artan atık üretiminin yarattığı zorluklara ve sürdürülebilir kalkınma zorunluluğuna çözüm bulmak için umut verici bir çözüm ve farkındalık sunmaktadır.

Anahtar kelimeler: Asfalt betonu, Seramik keki, Atık geri dönüşümü, Marshall tasarımı, Sürdürülebilir malzemeler

*Corresponding author

Plagiarism Checks: Yes – Turnitin
Complaints: fujece@firat.edu.tr

1. Introduction

Asphalt concrete pavements are the preferred choice in road networks due to their performance and ease of maintenance. This composite material primarily consists of aggregates and bitumen. Despite bitumen comprising only around 5% of asphalt concrete by proportion, it accounts for a substantial 80% to 90% of the total cost. In contrast, while aggregates constitute just 10-20% of the total cost, they make up approximately 95% of the composition of asphalt concrete. Even though the bitumen content in Hot Mix Asphalt (HMA) may be relatively low, it plays a pivotal role in determining overall coating performance [1-5].

On the other hand, the growth of industrial production has been accompanied by a relentless increase in waste generation, posing significant challenges to the environment. This surge in waste production has been driven by the global demand for products and services, resulting in higher levels of consumption and manufacturing. However, this intensified industrial activity has strained the availability of natural resources and the capacity of storage facilities. As a consequence, there has been a growing recognition of the urgent need to address the environmental repercussions of this burgeoning waste generation. The ever-mounting piles of waste have been associated with issues such as pollution, habitat degradation, and resource depletion. Additionally, the inadequacy of storage areas and the potential risks they pose to the environment have heightened concerns. In response to these pressing environmental concerns, a paradigm shift has occurred in research and industry practices. Waste management strategies have transitioned from conventional disposal methods to an emphasis on waste reduction, reuse, and recycling. This paradigm shift reflects a global commitment to sustainable practices that prioritize minimizing waste, conserving resources, and mitigating the environmental impact of waste disposal. This shift towards sustainable waste management practices has gained paramount importance across various sectors, including the construction industry and, notably, road construction. As a vital part of infrastructure development, the road construction sector has embraced the principles of sustainability, exploring innovative ways to incorporate recycled and repurposed materials into its processes. Research endeavors in this domain have not only sought to address waste challenges but have also aimed to optimize the performance and longevity of construction materials while minimizing their environmental footprint. [1-10].

Environmental waste materials find applications in asphalt concrete production, both in evaluating their potential in road construction and enhancing asphalt concrete's performance properties. These studies can be in the form of modified asphalt concrete mix [11-13] or modified bitumen [14-16]. The amount of material used in the mixture modification is higher than the bitumen modification. For this reason, environmental wastes can be evaluated at higher rates in the mixture modification of asphalt concrete. The amount of modifier used in bitumen modification is less. These additives can be used in the form of industrial production or as environmental waste [16, 17]. While industrial production materials tend to increase the production cost of asphalt concrete, the incorporation of environmental wastes generally reduces costs [3, 17-20].

For instance, Kara and Karacasu examined the effects of fully mixed ceramic waste on the mechanical behavior of HMA, revealing that as waste content increases, optimum bitumen content (OBC), voids in mineral aggregate (VMA), and void ratio (V) values increase, while Marshall Stability (MS), voids filled with asphalt or bitumen (VFA), and specific gravity (SG) values decrease [20].

This study investigates the feasibility of utilizing waste cake ceramics from ceramic factories in the Inonu region of Eskisehir, Turkey, in asphalt concrete production (Figure 1). The scope of this study encompasses a particular subset of waste materials generated within ceramic factories, which typically manifest in various forms, including waste generated from floors, walls, and ceramic cakes. It is essential to note that our investigation runs in parallel with three distinct master's studies, each specifically dedicated to exploring the utilization of one of these three aforementioned waste categories. The comprehensive exploration of these waste materials collectively forms a vital part of our commitment to sustainable practices within the ceramic industry. By sharing insights from this specific facet of our research, we aim to contribute valuable data and insights to the international literature, further enriching the body of knowledge on waste repurposing in construction.

Throughout our study, we systematically assessed the potential of ceramic cake waste (CCW) in asphalt concrete by replacing a portion of the aggregate material with CCW in varying proportions, including 10%, 20%, 30%, and 40% of

the aggregate weight. These substitutions were made in accordance with the corresponding grain sizes of the aggregate. The results obtained from these experiments provide critical insights into the feasibility and performance implications of integrating CCW into asphalt concrete mixtures, shedding light on its potential as a sustainable and cost-effective construction material.

Figure 1. Ceramic waste materials

2. Material and Method

Prior to delving into the methodological aspects of our study, it is essential to thoroughly understand the properties of the materials used and the characteristics of the test samples. In Table 1, we provide a comprehensive overview of the properties of the bitumen employed in our experiments, highlighting key parameters that play a significant role in the performance of asphalt concrete. Table 2 offers the analysis of the properties of the limestone aggregates utilized in our research, shedding light on their essential attributes.

Table 1. Properties of the bitumen used in the study

Properties	**Value**	**Standard**
Penetration (25°C, 100 g)	64	ASTM D5
Softening point (°C)	48	ASTM D36/D36M-09
Ductility (25°C, 5 cm/min)	>100 cm	ASTM D113-07
Loss of Heating (%)	0.430	ASTM D6-95
Flash Point (°C)	314	ASTM D92-05a
Specific Gravity (g/cm^3)	1.026	ASTM D70-09e1
Viscosity (at 135°C, cP)	437.5	ASTM D4402-06
Viscosity (at 165°C, cP)	137.5	ASTM D4402-06

Table 2. Properties of the aggregates used in the study

Properties	**Value**	**Standard**
Apparent specific gravity (g/cm^3) of coarse aggregate (CA)	2.709	ASTM C127, C128
Specific gravity (g/cm^3) of coarse aggregate (CA)	2.695	ASTM C127, C128
Saturated surface dry gravity (g/cm^3) of coarse aggregate (CA)	2.691	ASTM C127, C128
Apparent specific gravity (g/cm^3) of fine aggregate (FA)	2.858	ASTM C127, C128
Specific gravity (g/cm^3) of fine aggregate (FA)	2.727	ASTM C127, C128
Saturated surface dry gravity (g/cm^3) of fine aggregate (FA)	2.688	ASTM C127, C128
Specific gravity (g/cm^3) of filler (MF)	2.783	ASTM C127, C128
Water Absorption (%)	0.380	ASTM C127, C128
Compacted Bulk Density (g/cm^3)	1.572	ASTM C 29
Loose Bulk Density (g/cm^3)	1.301	ASTM C 29
Los Angeles Abrasion Test (%)	16.200	ASTM C 131
Flatness Index (%)	16	ASTM D 4791
Freeze-Thaw Resistance (%)	4	ASTM C 88

The aggregate material was designed to meet the limits for Marshall Mix Design (MMD) for wearing course type 2 in the Republic of Turkey General Directorate of Highways Technical Specification (HTS) and Superpave Mix Design (SMD) [21, 22]. The design and sieve analysis of the aggregate is given in Table 3.

Table 3. The design and sieve analysis of aggregate

						MMD		**SMD**	
Aggregate Type	**Sieve No (in)**	**Sieve (mm)**	**Size**	**$X^{0.45}$**	**Passing (%)**	**Lower Limit**	**Upper Limit**	**Lower Limit**	**Upper Limit**
CA	3/4"	19.000		3.76	**100**	*100*	*100*	*100*	*100*
CA	1/2"	12.500		3.12	**94**	*100*	*100*	*90*	*100*
CA	3/8"	9.500		2.75	**80**	*80*	*100*	-	-
CA	# 4	4.750		2.02	**49**	*55*	*72*	-	-
FA	# 8	2.360		1.47	**34**	-	-	*47.2*	*47.2*
FA	# 10	2.000		1.37	**31**	*36*	*53*	*36.8*	*42.4*
FA	# 16	1.180		1.08	**24**	-	-	*31.6*	*37.6*
FA	# 30	0.600		0.79	**18**	-	-	*23.5*	*27.5*
FA	# 40	0.425		0.68	**16**	*16*	*28*	*21.1*	*23.8*
FA	# 50	0.300		0.58	**14**	-	-	*18.7*	*18.7*
FA	# 80	0.180		0.46	**11**	*8*	*16*	-	-
FA	# 100	0.150		0.43	**10**	-	-	-	-
MF	# 200	0.075		0.31	**5.5**	*4*	*8*	-	-

CCW is a byproduct obtained through the filtration of production sludge, with residual moisture content ranging from approximately 28% to 32%. To meet the grain size requirements for asphalt concrete aggregate, we sieved the CCW waste material using a 1.18 mm sieve. Images of the samples can be found in Figure 2, while characteristics of CCW waste and XRF analysis results are detailed in Tables 4 and 5, respectively.

Figure 2. CCW samples

Table 4. Properties of the CCW used in the study

Properties	**Value**
Dry Strength (kg/cm3)	5.40
Cooked Size (mm)	89.95 x 179.85
Total Firing Shrinkage (%)	10.06
Baked Strength (kg/cm3)	464.50
Compacted Bulk Density (g/cm^3)	1.471
Loose Bulk Density (g/cm^3)	1.298
Water Absorption (%)	31.64
Black Core	NA
Color – L	54.45
Color – A	2.76
Color – B	10.09

Table 5. XRF analysis of CCW used in the study

Report Name	**Result**	**Report Name**	**Result**
L.O.I (%)	5.795	Na_2O	0.378
SrO (%)	0.021	SiO_2	63.510
ZrO_2 (%)	0.738	P_2O_5	0.132
NiO (%)	0.030	CuO	1.896
ZnO(%)	0.675	Al_2O_3	18.304
BaO (%)	0.171	SO_3	0.079
PbO (%)	0.014	TiO_2	0.661
Fe_2O_3 (%)	1.699	Cr_2O_3	0.024
CeO_2 (%)	0.155	K_2O	1.835
HfO_2 (%)	0.133	CaO	3.748

In our study, we employed the globally recognized MMD method for asphalt concrete [23-30]. We prepared a total of 105 asphalt concrete samples for our study, encompassing both control and ceramic cake waste (CCW)-containing specimens. Bitumen content in the samples ranged from 3.5% to 6.5%, with increments of 0.5%, resulting in 21 different ratios. For each ratio, we produced three samples. These specimens, totaling 105, consisted of 1150 grams of aggregate mixed with bitumen at a temperature of 160°C. Following the sample preparation, we subjected each specimen to 75 impacts on both surfaces using an automatic Marshall impact compactor, meeting EN 12697-30, 12697-10, 12697-12, ASTM D 1559, ASTM D 6926; AASHTO T245 standards. Subsequently, we measured specimen heights and subjected them to destructive testing. For this purpose, we utilized an Automatic Marshall Stability Test Machine, meeting EN 12697-34, 12697-23, 12967-12 (A), ASTM D1559, D5581, D6927; D6931; AASHTO T245, T283, EN 12697-44; NF P98-251-2 standards, to determine the Marshall Stability and flow values. Our analysis encompassed key parameters such as Marshall Stability (MS), flow (F), practical specific gravity (PSG), and void properties, including void ratio (V), voids in mineral aggregate (VMA), and voids filled with asphalt or bitumen (VFA). These measurements were instrumental in determining the optimum bitumen content (OBC) for each sample. It's important to highlight that every sample in our study adhered to the defined control standards specified in the Highways Technical Specification (HTS), as detailed in Table 6.

Table 6. MMD criteria outlined in the HTS

Experiment Name	**Bitumen Content (BC) (%)**	
Layer Type	*Binder*	*Wearing*
Unit Weight (g/cm^3)	Max.	Max.
MS (kg)	Min. 750	Min. 900
V (%)	4-6	3-5
VFA (%)	60-75	65-75
VMA (%)	Min. 13	Min. 14
F (mm)	2-4	2-4

3. Test Results and Evaluation

OBC graphs for both control and CCW-containing samples are presented in Figure 3. It's evident that OBC increases with the addition of CCW when compared to standard asphalt concrete samples. This emphasizes the need for a comparative assessment of the cost of waste material usage versus bitumen usage and the importance of conducting a feasibility study in this regard.

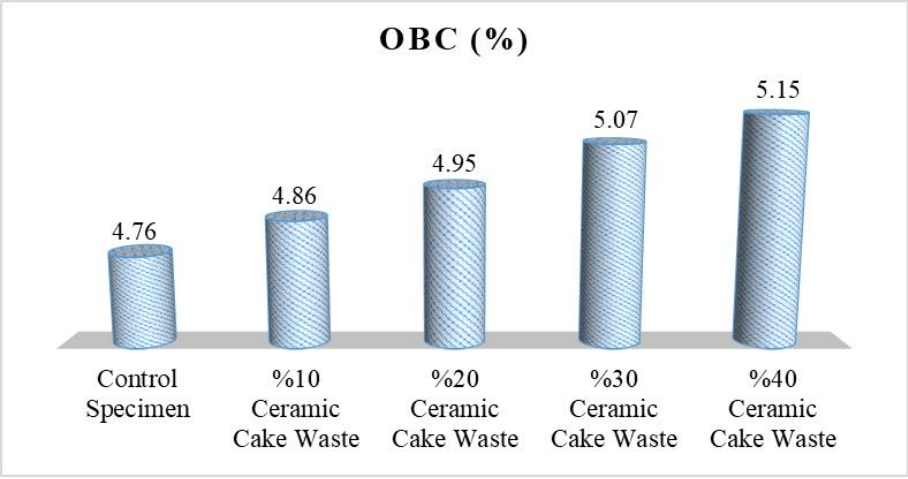

Figure 3. OBC values for each specimen type

The PSG values of CCW-containing samples are consistently lower than those of the control samples. This trend is directly linked to the increase in void ratio within the asphalt concrete as the CCW content rises, as illustrated in Figure 4. The porous nature of CCW contributes to this rise in void ratio, as demonstrated in Figure 5.

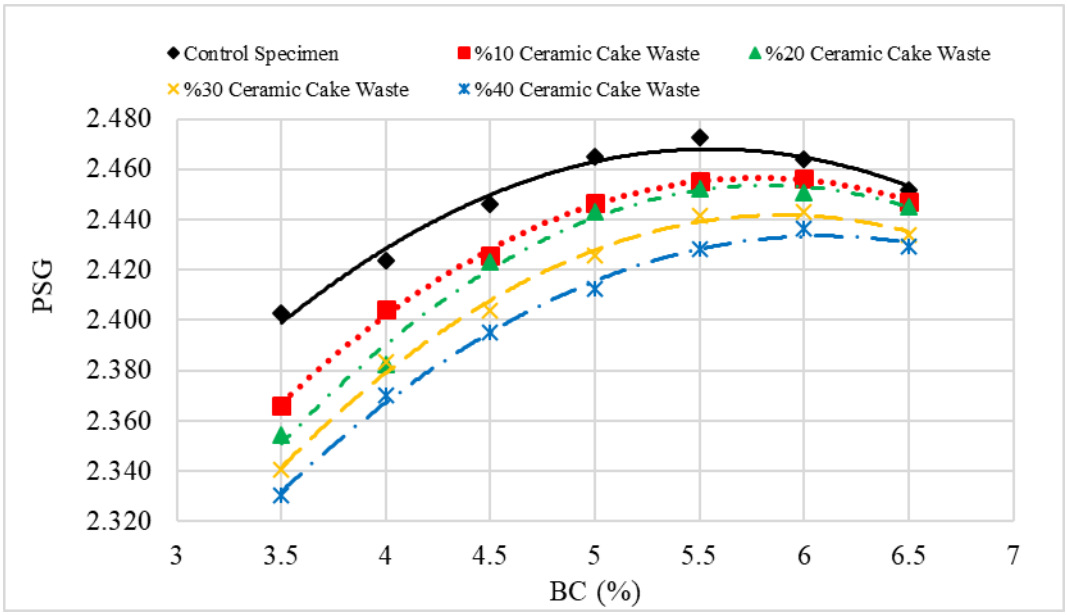

Figure 4. PSG and BC curves graph for each specimen type

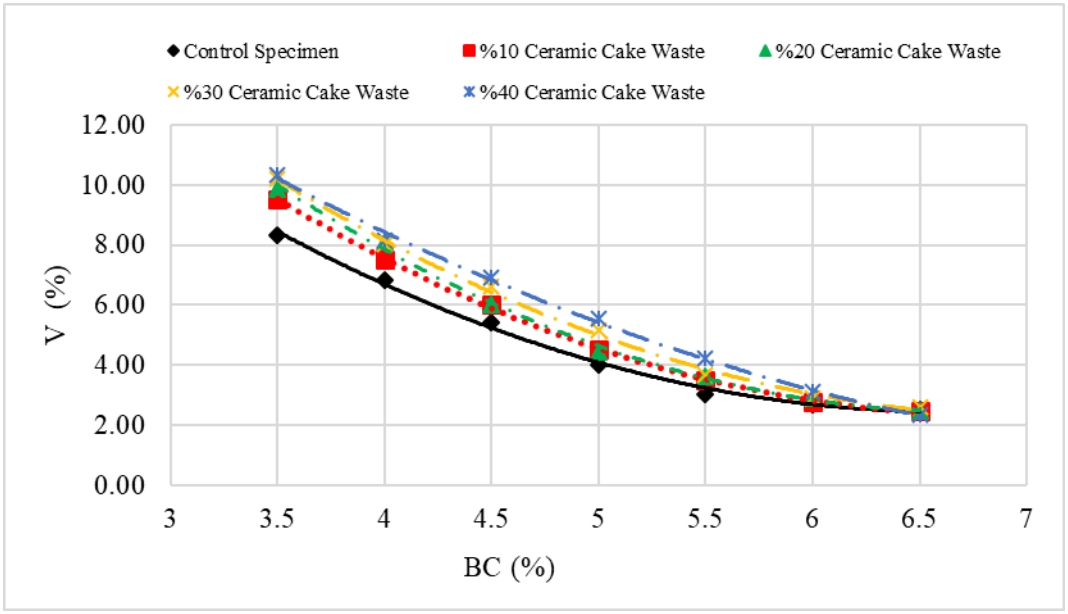

Figure 5. V and BC curves graph for each specimen type

As the BC increased, there was a corresponding increase in VFA. However, according to our experimental results, VFA values exhibited a decrease as the CCW ratio increased, as shown in Figure 6. Additionally, MS was lower in CCW-containing samples compared to control samples, indicating a decrease in stability associated with the increased void ratio due to the presence of CCW materials, as depicted in Figure 7.

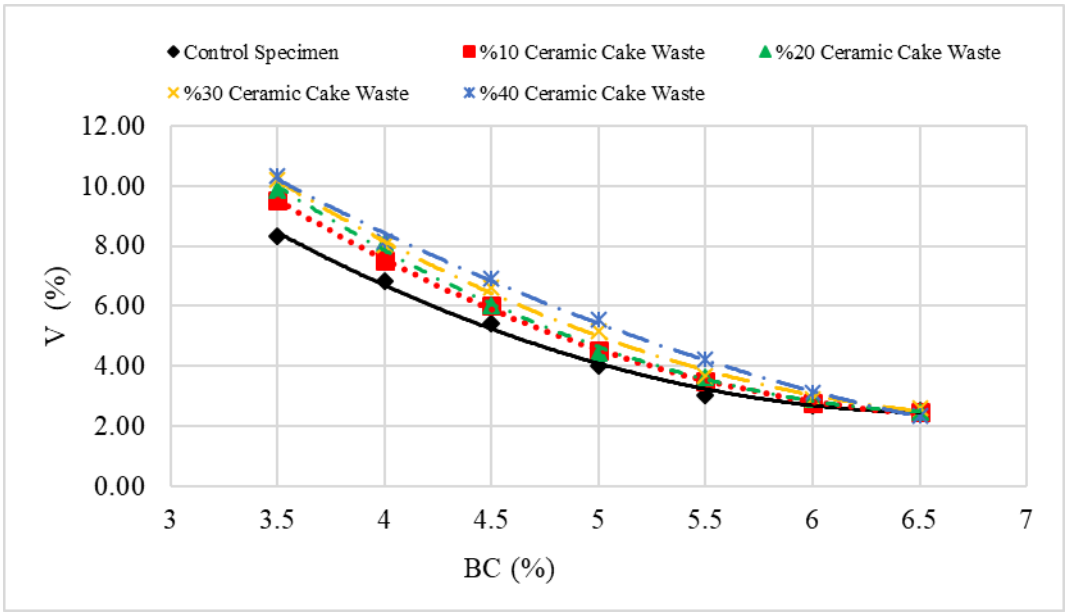

Figure 6. V and BC curves graph for each specimen type

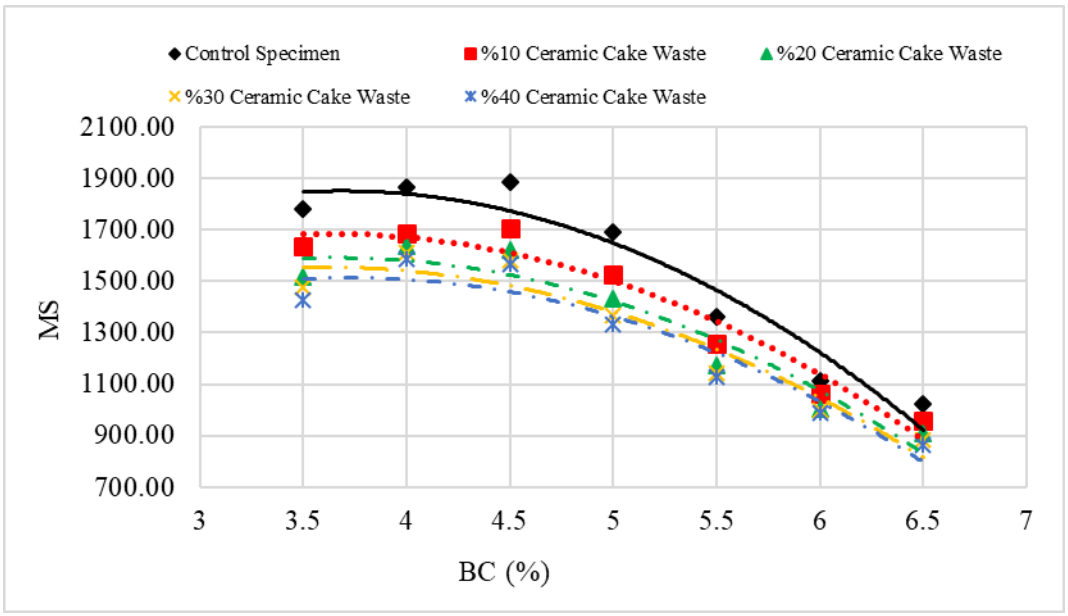

Figure 7. MS and BC curves graph for each specimen type

F values can vary due to sample manufacturing and grain distribution. In samples containing waste, F values are comparable to those of control samples, and all values fall within specification limits, as shown in Figure 8. Marshall Quotient (MQ), expressed as the ratio of MS to F (MS/F), serves as a stiffness indicator for the samples. Higher MQ values are preferred. However, CCW-containing samples exhibit lower MQ ratios than control samples, as illustrated in Figure 9. This trend in MQ correlates consistently with the MS results. Additionally, when examining VMA ratios in relation to BC, it's evident that all samples meet the lower specification limits (≥14%) for VMA, as depicted in Figure 10.

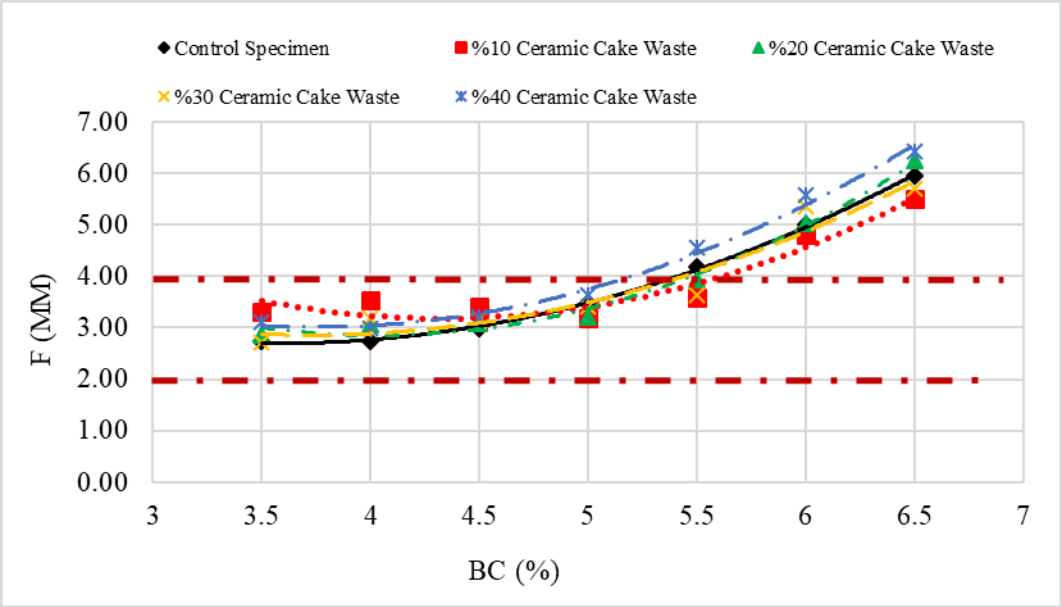

Figure 8. F and BC curves graph for each specimen type

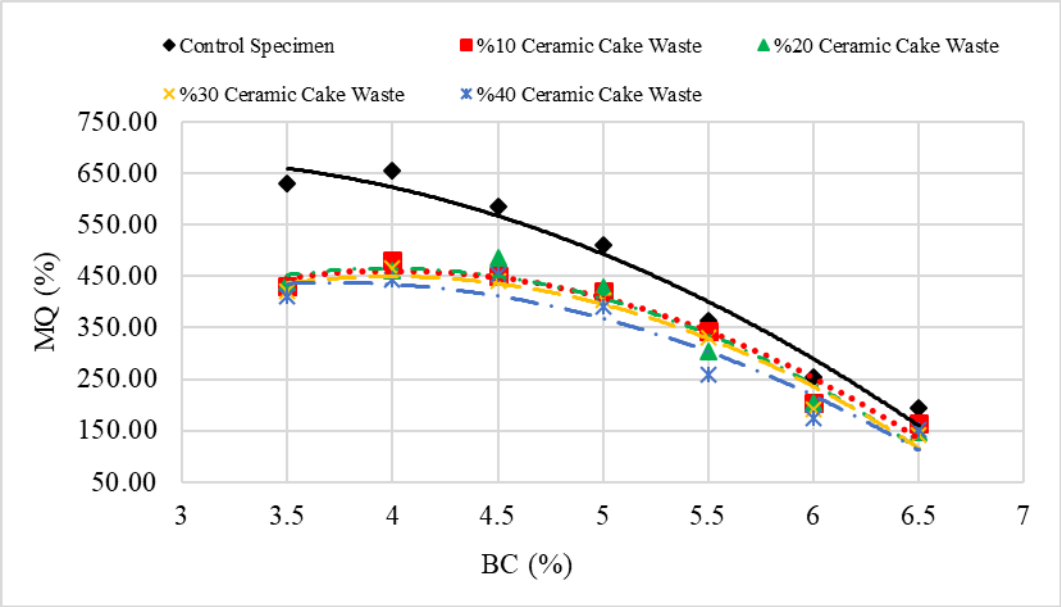

Figure 9. MQ and BC curves graph for each specimen type

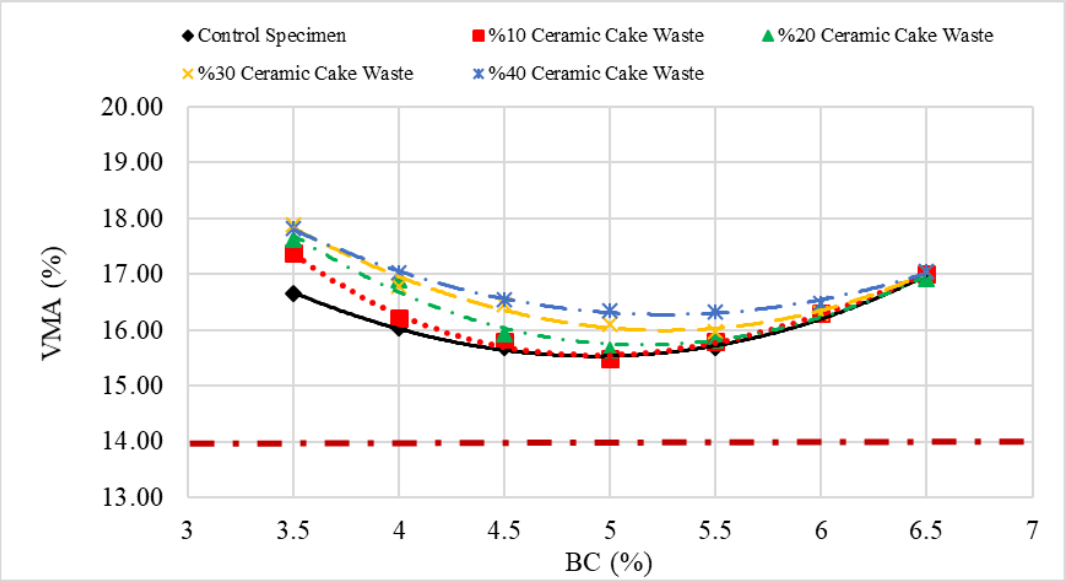

Figure 10. VMA and BC curves graph for each specimen type

In the field of incorporation of waste materials into asphalt concrete, our study extends and supports the findings of two previously conducted research studies. Our experimental results consistently corroborate the findings of these earlier studies. These research efforts have highlighted the benefits of integrating ceramic waste into asphalt mixtures, demonstrating that performance standards can be met by substituting recycled ceramic waste for up to 20% in the wearing course and 30% in the binder course [20, 31].

4. Conclusion

This comprehensive study delved into the feasibility of utilizing ceramic cake waste (CCW) materials in the production of asphalt concrete, a critical component of road construction. To gain a thorough understanding of the implications of CCW incorporation, we meticulously prepared and subjected a total of 105 asphalt concrete samples to an array of tests.

Our investigation unearthed several noteworthy trends that shed light on the impact of CCW on asphalt concrete properties. As the CCW content increased within the mixture, we observed corresponding increases in key parameters such as void ratio (V), voids in mineral aggregate (VMA), flow (F), and optimum bitumen content (OBC). Conversely, values for Marshall Stability (MS), practical specific gravity (PSG), voids filled with asphalt or bitumen (VFA), and Marshall Quotient (MQ) exhibited a consistent decrease with higher levels of CCW.

In particular, one of the most significant findings of our study is the identification of an optimal 20% CCW content for wearing course that aligns harmoniously with the Republic of Turkey General Directorate of Highways Technical Specification. This specific ratio not only meets the regulatory standards but also holds promise as a sustainable approach to road construction.

The broader significance of our research expands into the domains of environmental preservation and waste management. By promoting the reuse of ceramic cake waste in road construction, we effectively contribute to reducing both environmental and visual pollution. Simultaneously, our approach optimizes waste storage and maximizes resource utilization, underlining the importance of sustainable practices in modern infrastructure development.

In summation, our study underscores the potential for the responsible integration of ceramic cake waste in road construction, offering a compelling solution to the challenges posed by escalating waste generation and the imperative for sustainable development. These findings promote a greener, more sustainable future and a higher quality of life for the communities.

Future work in this field should focus on optimizing the CCW content within asphalt concrete, exploring the potential for variations beyond the 20% ratio. The potential applications of cake waste, especially those aimed at reducing OBC and enhancing MS through the use of various additives or waste combinations, warrant comprehensive examination. Apart from the Marshall Mix Design, it is advisable to consider investigations into Superpave Mix Design methodologies. Furthermore, conducting long-term performance assessments under diverse environmental conditions, rigorous environmental impact evaluations, and in-depth cost-benefit analyses are crucial steps. Expanding research to include alternative waste materials, exploring performance-enhancing additives, and establishing robust regulatory frameworks will propel the advancement of sustainable road construction practices. It is also important to engage with local communities and conduct comprehensive life cycle analyses to achieve a holistic assessment. Lastly, interdisciplinary research, integrating engineering, environmental science, economics, and policy studies, will furnish a comprehensive comprehension of the integration of waste materials into infrastructure projects, ultimately leading to more environmentally friendly and cost-effective road construction solutions.

5. Author Contribution Statement

The authors have no conflicts of interest to declare. All co-authors have seen and agree with the contents of the manuscript and there is no financial interest to report. We certify that the submission is original work and is not under review at any other publication.

6. Ethics Committee Approval and Conflict of Interest

“There is no conflict of interest with any person/institution in the prepared article”

7. References

[1] Abdulrasool AT, Kadhim YN, Hussain WAM, Kashesh GJ, Abdulhussein HA. "The effect of cow dung ash as a filler on the mechanical characteristics of hot mix asphalt". In IOP Conference Series: Earth and Environmental Science (Vol. 961, No. 1, p. 012041). IOP Publishing, 2022.

[2] Sang L, Idowu T, Okumu V. "Evaluation of the performance of waste marble dust as a mineral filler in hot-mix asphalt concrete". *Journal of Civil Engineering, Science and Technology*, 12(1), 1-14, 2021.

[3] Keskin M, Karacasu M. "Effect of boron containing additives on asphalt performance and sustainability perspective". *Construction and Building Materials*, 218, 434-447, 2019.

[4] Khan D, Khan R, Khan MT, Alam M, Hassan T. "Performance of hot-mix asphalt using polymer-modified bitumen and marble dust as a filler". *Journal of Traffic and Transportation Engineerin*g (English Edition), 2023.

[5] Ming NC, Jaya RP, Awang H, Ing NLS, Hasan MRM, Al-Saffar ZH. "Performance of glass powder as bitumen modifier in hot mix asphalt". Physics and Chemistry of the Earth, Parts A/B/C, 128, 103263, 2022.

[6] Jiang W, Bao R, Lu H, Yuan D, Lu R, Sha A, Shan J. "Analysis of rheological properties and aging mechanism of bitumen after short-term and long-term aging". *Construction and Building Materials*, 273, 121777, 2021.

[7] Raschia S, Tattolo S. "Use of alternative aggregates for the production of hot-mix asphalt surface layers: A performance evaluation". Construction and Building Materials, 345, 128369, 2022.

[8] Yaro NSA, Sutanto MH, Habib NZ, Napiah M, Usman A, Al-Sabaeei AM, Rafiq W. "Feasibility evaluation of waste palm oil clinker powder as a fillers substitute for eco-friendly hot mix asphalt pavement". *International Journal of Pavement Research and Technology*, 1-14, 2022.

[9] Babalghaith AM, Koting S, Sulong NHR, Khan MZH, Milad A, Yusoff NIM, Ibrahim MR, Mohamed AHBN. "A systematic review of the utilization of waste materials as aggregate replacement in stone matrix asphalt mixes". *Environmental Science and Pollution Research*, 29(24), 35557-35582, 2022.

[10] Luo Y, Zhang K. "Review on performance of asphalt and asphalt mixture with waste cooking oil". *Materials*, 16(4), 1341, 2023.

[11] Yaro NSA, Sutanto MH, Baloo L, Habib NZ, Usman A, Yousafzai AK, Ahmad A, Birniwa AH, Jagaba AH, Noor A. "A comprehensive overview of the utilization of recycled waste materials and technologies in asphalt pavements: towards environmental and sustainable low-carbon roads". *Processes*, 11(7), 2095, 2023.

[12] Ali AM, Al-Mansoori T. "Investigation of asphalt binder performance modified with ceramic waste powder". In IOP Conference Series: *Materials Science and Engineering*, 1090, 1. IOP Publishing, 2021.

[13] Fatima E, Sahu S, Jhamb A, Kumar R. "Use of ceramic waste as filler in semi-dense bituminous concrete". *American Journal of Civil Engineering and Architecture*, 2(3), 102-106, 2014.

[14] Gülşah ÖZ, Saltan M. "Pirinanın Bitüm Modifikasyonunda Kullanımının araştırılması". *International Journal of Technological Sciences*, 12(1), 2020.

[15] Cao W. "Study on properties of recycled tire rubber modified asphalt mixtures using dry process". *Construction and building materials*, 21(5), 1011-1015, 2007.

[16] Kaçaroğlu G, Saltan M. "Cocamide diethanolamide kimyasalının bitüm modifikasyonunda kullanımı". *Pamukkale University Journal of Engineering Sciences*, 26(6), 1042-1047, 2020.

[17] Sanchez-Cotte EH, Fuentes L, Martinez-Arguelles G, Quintana HAR, Walubita LF, Cantero-Durango JM. "Influence of recycled concrete aggregates from different sources in hot mix asphalt design". *Construction and Building Materials*, 259, 120427, 2020.

[18] Kök BV, Yılmaz M, Kuloğlu N. "Asfaltit ve SBS Modifiyeli Bitümlü Sıcak Karışımların Mekanik Özelliklerinin Değerlendirilmesi". *Journal of Polytechnic*, 14(3), 193-197, 2011.

[19] Wu S, Montalvo L. "Repurposing waste plastics into cleaner asphalt pavement materials: A critical literature review". *Journal of Cleaner Production*, 280, 124355, 2021.

[20] Kara Ç, Karacasu M. "Use of ceramic wastes in road pavement design". In Proceedings of the world congress on new technologies. Barcelona, Spain (pp. 226-6), 2015.

[21] Republic of Turkey General Directorate of Highways. "Highways Technical Specification". Ankara, 2013.

[22] Asphalt Institute. "Superpave Mix Design". Superpave Series No 2, 56, Lexington, 1996.

[23] Atakan M, Yıldız K. "Prediction of Marshall design parameters of asphalt mixtures via machine learning algorithms based on literature data". *Road Materials and Pavement Design*, 1-20, 2023.

[24] Awan HH, Hussain A, Javed MF, Qiu Y, Alrowais R, Mohamed AM, Fathi D, Alzahrani AM. "Predicting marshall flow and marshall stability of asphalt pavements using multi expression programming". *Buildings*, 12(3), 314, 2022.
[25] Kandhal PS, Koehler WS. "Marshall mix design method: current practices". In Association of Asphalt Paving Technologists Proc (Vol. 54), 1985.
[26] Karacasu, M. "Yol Üstyapı Deneyleri". Sözkesen Matbaacılık Ltd. Şti,, Ankara, 2016.
[27] Khodadadi M, Moradi L, Dabir B, Nejad FM, Khodaii A. "Reuse of drill cuttings in hot mix asphalt mixture: A study on the environmental and structure performance". *Construction and Building Materials*, 256, 119453, 2020.
[28] Tapkın S, Çevik A, Uşar Ü. "Prediction of Marshall test results for polypropylene modified dense bituminous mixtures using neural networks". Expert Systems with Applications, 37(6), 4660-4670, 2010.
[29] Wan L, Garcia-Hernández A, Cui G, Liu P. "A novel performance-based method to design asphalt mixtures". *Construction and Building Materials*, 400, 132792, 2023.
[30] White TD. "Marshall procedures for design and quality control of asphalt mixtures". In Association of asphalt paving technologists proc, 54, 1985.
[31] Kara Ç, Karacasu M. "Investigation of waste ceramic tile additive in hot mix asphalt using fuzzy logic approach". *Construction and Building Materials*, 141, 598-607, 2017.

Firat Univ Jour. of Exp. and Comp. Eng., 2(3), 117-123, 2023

Firat University Journal of Experimental and Computational Engineering
Fırat Üniversitesi Deneysel ve Hesaplamalı Mühendislik Dergisi

Damage Assessment of Masonry Structures in Adıyaman Province After Kahramanmaraş Earthquakes (February 6, 2023)

Kahramanmaraş Depremleri Sonrası Adıyaman İlindeki Yığma Yapıların Hasar Değerlendirmesi (6 Şubat 2023)

Ertuğrul ÇAMBAY[1]*

[1]Department of Civil Engineering, Faculty of Engineering - Architecture, Bitlis Eren University, Bitlis, Turkey
[1]ecambay@beu.edu.tr

Received: 01.08.2023
Accepted: 29.09.2023
Revision:15.09.2023
doi: 10.5505/fujece.2023.47955
Research Article

Citation: Çambay E. "Damage assessment of masonry structures in adıyaman province after kahramanmaraş earthquakes (February 6, 2023)". *Firat University Journal of Experimental and Computational Engineering*, 2(3), 117-123, 2023.

Abstract
According to the data of the Disaster and Emergency Management (AFAD) Earthquake Department; On February 6, 2023, at 4.17 and 13.24 Turkey time, earthquakes with magnitudes of 7.7 and 7.6 (Mw) occurred, respectively, with the epicenters in Pazarcık (Kahramanmaraş) and Elbistan (Kahramanmaraş). These earthquakes affected 11 provinces of Turkey and were recorded as the most destructive earthquakes in the last century. In the statement made by AFAD on April 20, 2023, it was reported that the number of people who lost their lives in the earthquakes centered in Kahramanmaraş was 50 thousand 96 and the number of people injured was 107 thousand 204. Adıyaman was shaken by the effects of the earthquakes and many buildings were destroyed and damaged. In this study, after the earthquakes, some damaged masonry structures, and in fill walls in Adıyaman city center; the structural irregularities, application methods and material properties used were examined on site and the causes of the damages were evaluated. The damages suffered by historical buildings in the earthquake as a result of the strengthening were discussed. After the buildings were demolished, on-site inspections were carried out.

Keywords: Earthquake, Damage evaluation, Masonry buildings

Özet
Afet ve Acil Durum Yönetimi (AFAD) Deprem Dairesi Başkanlığı verilerine göre; 6 Şubat 2023 tarihinde Türkiye saati ile 4.17 ve 13.24'te merkez üsleri Pazarcık (Kahramanmaraş) ve Elbistan (Kahramanmaraş) olan sırasıyla 7.7 ve 7.6 (Mw) büyüklüklerinde depremler meydana geldimiştir. Bu depremler Türkiye'nin 11 ilini etkilemiş ve son yüzyılın en yıkıcı depremleri olarak kayıtlara geçmiştir. AFAD tarafından 20 Nisan 2023 tarihinde yapılan açıklamalarda, Kahramanmaraş merkezli depremlerde hayatını kaybedenlerin sayısının 50 bin 96, yaralananların sayısının ise 107 bin 204 olduğu bildirilmişti. Depremlerin etkisiyle sarsılan Adıyaman'da çok sayıda bina yıkıldı ve hasar görmüştür. Bu çalışmada, depremler sonrasında Adıyaman şehir merkezinde hasar gören bazı yığma yapılar ve dolgu duvarlar; yapısal düzensizlikler, uygulama yöntemleri ve kullanılan malzeme özellikleri açısından yerinde incelenmiş ve hasarların nedenleri değerlendirilmiştir. Tarihi yapıların güçlendirme işlemi sonucunda depremden aldığı hasarlar değerlendirilmiştir. Yıkım gerçekleştikten sonar yerinde incelemelerde bulunulmuştur.

Anahtar kelimeler: Deprem, Hasar tespiti, Yığma binalar

1. Introduction

Turkey is located on the North Anatolian Fault, East Anatolian Fault, Northeast Anatolian Fault and West Anatolian Fault. North Anatolian and East Anatolian Faults are the most active faults. The earthquakes that have occurred in Turkey in recent years are caused by these two faults but have resulted in significant loss of life and high amounts of structural damage.

*Corresponding author

It is possible to see this situation in many historical buildings due to the major earthquakes that occurred in our country, which is the earthquake zone. Masonry structures can easily transfer their own weight and vertical forces such as dead and live loads to their foundation systems. However, they are weak in transferring tensile stresses that occur under horizontal loads such as earthquakes. Masonry building elements that exhibit brittle behavior under tensile stresses can collapse under earthquake loads and cause heavy loss of life and property [1-4].
Masonry walls are important structural elements used as carriers or as filling units in frames. In framed and/or sheared systems, masonry walls used as filling units contribute positively to the behavior of the system under earthquake loads. Since these building elements are constructed from brick/stone and binding materials, they are considered a composite material. Masonry walls, which exhibit a complex behavior with this feature, continue to exist as the most preferred building element today.

According to the data of the Disaster and Emergency Management (AFAD) Earthquake Department; On February 6, 2023, earthquakes with magnitudes of 7.7 and 7.6 (Mw) occurred at 4.17 and 13.24 Turkey time, with the epicenters in Pazarcık (Kahramanmaraş) and Elbistan (Kahramanmaraş), respectively. These earthquakes affected 11 provinces of Turkey and were recorded as the most destructive earthquakes in the last century. In the statement made by AFAD on April 20, 2023, it was reported that the number of people who lost their lives in the earthquakes centered in Kahramanmaraş was 50 thousand 96 and the number of people injured was 107 thousand 204.

In this study, damage assessment studies were carried out in Adıyaman city center between February 10-17, 2023, and the effects of the earthquake forces on the masonry structures in the region were examined on-site. According to the data taken from the seismometers at the central station no 0201 in Adıyaman province during the first earthquake, the largest ground acceleration values were obtained as 0.383 g in the east-west direction and 0.281 g in the North-South direction. Acceleration-time graphs of the stations in question are given in Fig 1.

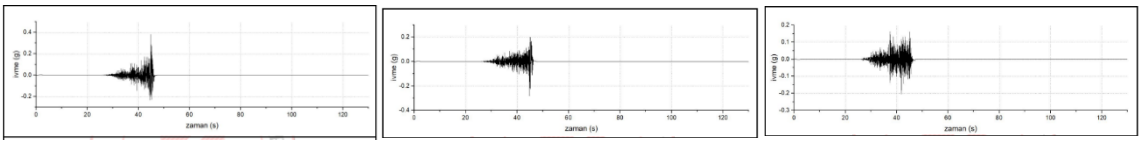

a) East-west (0.383g) b) North-South (0.281g) c) Up-down (0.206g)

Figure 1. Acceleration graphs of Adıyaman Central Station No. 0201 [5]

2. Behavior of masonry structures

It was determined that the most damage in masonry structures in the earthquake zone occurs out of the plane, or in other words, as a result of the first damage mode (Fig 2). It was also observed that beam connection elements are missing in the majority of damaged structures. Şenol [6] damage assessment studies were carried out in Antakya and İskenderun districts of Hatay province between 20-23 February 2023, and the structures in the region; It was examined on-site in terms of structural irregularities, materials used and the effect of earthquake forces. Tomazevic [7] pointed out that as a result of the out-of-plane behavior of masonry walls, cracks may occur in the regions where stress concentrations are most intense and, as a result, collapses in the direction perpendicular to the direction of seismic movement. Subsequently, Ayala and Speranza [8] concluded that the out-of-plane behavior of walls and the collapses that occur as a result of this behavior are directly proportional to the quality and strength of the connections and wall elements.

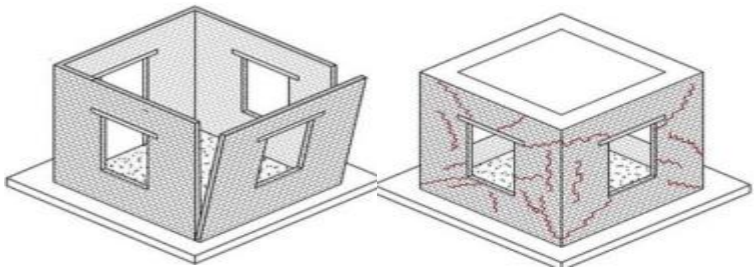

a) b)

Figure 2. a) Out-of-plane behavior b) In-plane behavior [9]

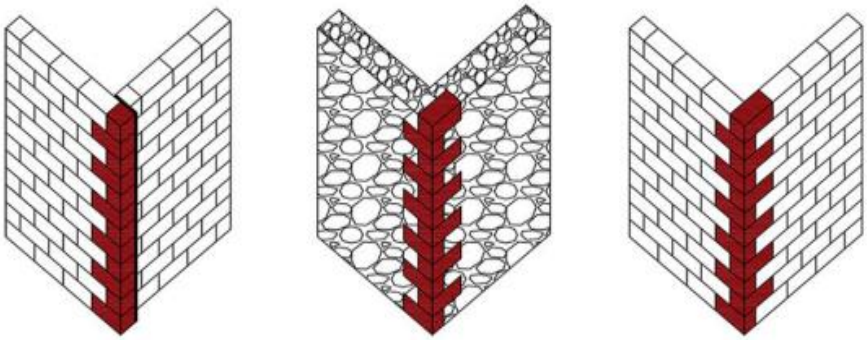

a) b) c)

Figure 3. Corner details: (a) Lack of keystone, (b) Insufficient support c) a sufficient combination. [9]

Corner joint damages were frequently encountered in studies carried out in the earthquake zone. roper wall-to-wall and wall-to-floor connections this construction increases the strength of the corners under the influence of earthquakes (Fig 3).

3. Damage Observations

After the restoration process in 2021, the Adıyaman Tuz Hanı, built in the 1800s, was observed to have suffered major damage as a result of the 6 February Pazarcık earthquake. As a result of on-site inspections, damage occurred due to out-of-plane behavior. In particular, it has been determined that the masonry units were built using randomly placed stones with irregular shapes. The lack of sufficient connections between stones has resulted in poor earthquake performance of such structures. TDY [10], to increase the lateral resistance of masonry structures against earthquakes, it is mandatory to use reinforced beam systems called both horizontal and vertical beams. However, no reinforced concrete beams were seen on the exterior of this building (Fig. 4). As a result of the restoration, careless workmanship and random placement of stones were also determined as a result of the examinations.

Figure 4. Tuz Hanı in the center of Adıyaman

As a result of field studies carried out in the region, it was observed that most of the masonry structures were built using a mixture of natural stone and perforated clay bricks. Due to the weakness and brittleness of the perforated clay brick material, it has been concluded that the seismic behavior of masonry structures built using this type of material is weak. In many cases, it has been found that under the influence of earthquakes, clay elements lose their strength before mortar. Generally, it has been found that clay bricks are crushed as soon as masonry walls begin to lose their strength due to shearing. This loss in the connection between masonry materials can lead to collapse following the initiation of cracks. The fact that the infill wall of the reinforced concrete building was manufactured without being compressed between columns caused both in-plane and out-of-plane behavior (Fig 5).

Figure 5. Damaged masonry walls in Adıyaman city center

Figure 6. Kap mosque in the center of Adıyaman

It was observed that the lack of connection between the roof and walls in the mosque under investigation increased the earthquake damage. In many historical buildings in the region, the roofs are made of wooden beams and are supported directly on the load-bearing walls. Failure to install beam systems at the roof level disrupts the box behavior of the masonry structure, causing masonry walls to collapse in out-of-plane directions. Fig-6 shows the earthquake damages observed as a result of the roof system not being supported correctly to the walls.

In addition, corner joint damages were frequently encountered in studies carried out in the earthquake zone. It has been shown in the literature that lateral stresses caused by the roof increase the damage. Improper wall-to-wall and wall-to-floor connections reduce the strength of corners under earthquake effects. In particular, incorrect support of corner joints causes them to become unstable. In case of roof damage, non-deformed walls usually topple over, causing major damage. The quality of the wall is determined by the effectiveness of the keystones used. Fig. 7 shows the corner joint damages observed in the region.

Figure 7. Damaged masonry walls in Adıyaman city center

Although some of the reinforced concrete buildings in the region survived this devastating earthquake with little or no damage, it is possible to observe wall damage in most of these structures [11]. They are generally detected as diagonal shear cracks. Walls moving out of the plane and walls detached from the frame system have also been observed. Due to the weakness and brittleness of the perforated brick material, it has been concluded that the seismic behavior of masonry structures built using this type of material is weak. In many cases, it has been found that under the influence of earthquakes, clay elements lose their strength before mortar. Generally, it has been found that clay bricks are crushed as soon as masonry walls begin to lose their strength due to shearing. This loss in the connection between masonry materials can lead to collapse following the initiation of cracks. Perforated clay brick elements were used and infill walls that were damaged because adherence could not be achieved with the missing mortar are shown in Fig. 8.

Figure 8. Ulu mosque in the center of Adıyaman

Adıyaman Ulu Mosque, which is estimated to have been built in the 16th century, was destroyed except for its north-west walls by the February 6 earthquake. The mosque was determined that additional loads were placed on the structure as a result of the restoration work carried out in 2016. The mosque lost its historical texture.

4. Results

Disaster and Emergency Management (AFAD) Earthquake Department; On February 6, 2023, at 4.17 and 13.24 Turkey time, earthquakes with magnitudes of 7.7 and 7.6 (Mw) occurred, respectively, with the epicenters in Pazarcık (Kahramanmaraş) and Elbistan (Kahramanmaraş). Adıyaman was shaken by the effects of the earthquakes and many buildings were destroyed and damaged. After the earthquakes, some damaged masonry structures and infill walls in Adıyaman city center. Within this framework, the structural irregularities, application methods and material properties used were examined on site and the causes of the damages were evaluated.
According to the results obtained from the observations:

- It was concluded that the seismic behavior of unreinforced masonry structures exposed to horizontal and vertical load combinations depends on many parameters.
- As a result of the restoration, poor workmanship and the use of low-strength materials are the primary causes of the damages observed.
- In addition, it was observed that the mechanical properties of the material used for the restoration, loading conditions, the way the nodes are formed, construction technology and site conditions have direct effects on the seismic performance of the structure.
- It was also observed that building load-bearing walls without using beams and placing roofs directly on the walls makes the structures in the region prone to out-of-plane behavior.

5. Credit Authorship Contribution Statement

Ertuğrul ÇAMBAY: Conceptualization, Data curation, Formal analysis, Investigation, Methodology, Validation, Visualization, Writing – original draft, Writing - review & editing.

6. Ethics Committee Approval and Conflict of Interest

The authors declare that they have no known competing financial interests or personal relationships that could have appeared to influence the work reported in this paper.

7. References

[1] Çambay E. Yığma Yapıların Mikro Modellenmesinde Dönel Yayılı Hasar Modelinin Etkinliğinin İncelenmesi: Eindhoven Duvarları Örneği. PhD Thesis, Fırat University, Elazığ, Turkey, 2022.
[2] Karaton M, Çanakçı K. "Micro model analysis of JD6 and JD7 eindhoven walls with fixed smeared crack model", *Journal of Structural Engineering & Applied Mechanics*,3,2020.
[3] Lourenço N, Paulo B. "Current Experimental and Numerical Issues in Masonry Research". *Congresso Nacional de Sismologia Engenharia Sísmica*,119-136,2004.
[4] Ural A. Yığma Yapıların Doğrusal ve Doğrusal Olamayan Davranışlarının İncelenmesi, PhD Thesis, Karadeniz Technical University, Trabzon, 186, 2009.
[5] Şenol FA. "Kahramanmaraş Depremleri (6 Şubat 2023) Sonrası Hatay İlindeki Yapıların Hasar Durumlarının Değerlendirilmesi". 2nd International Conference on Engineering, Natural and Social Sciences, April 4-6 Konya, Turkey.
[6] Konya Teknik Üniversitesi. ''Pazarcik Mw=7.7 & Elbistan Mw=7.6 Depremleri Raporu (Hatay Bölgesi)'' Konya Teknik Üniversitesi, Konya, Türkiye, 2023.
[7] Tomazevic M. "Shaking table tests of small-scale models of masonry buildings: advantages and disadvantages". Massivbau 2000: Forschung, Entwicklungen, Anwendungen, 2000.
[8] Ayala DD, Speranza E. "Definition of collapse mechanisms and seismic vulnerability of historic masonry buildings". *Earthquake Spectra*, 19, 3, 479-509, 2003.
[9] RA Oyguç. "Van depremlerinden sonra yığma yapılarda gözlemlenen hasarlar", İstanbul Teknik Üniversitesi, Deprem Mühendisliği ve Afet Yönetimi Enstitüsü, Maslak, İstanbul, Türkiye, 2017.
[10] TDY, Deprem bölgelerinde yapılacak binalar hakkında yönetmelik, T.C. Bayındırlık ve İskan Bakanlığı, Ankara, Türkiye, 2007.
[11] Gebze Teknik Üniversitesi. ''6 Şubat 2023 Maraş Depremleri (Pazarcik Mw=7.7 ElbistanMw=7.6) Sonrasında Kuvvetli yer Hareketi, Geoteknik Üst yapı ve altyapılara ilişkin Saha Gözlemleri'' Gebze Teknik Üniversitesi, Martest Kocaeli, Türkiye, 2023.
[12] Qi K, Liu S, Chen Y, Xia B, Li GD. "A simple post-treatment with urea solution to enhance the photoelectric conversion efficiency for TiO_2 dye-sensitized solar cells". *Solar Energy Materials and Solar Cells*, 183, 193-199, 2018.

Firat Univ Jour. of Exp. and Comp. Eng., 2(3), 124-133, 2023

Firat University Journal of Experimental and Computational Engineering
Fırat Üniversitesi Deneysel ve Hesaplamalı Mühendislik Dergisi

Testing The Performance of Random Forest and Support Vector Machine Algorithms for Predicting Cyclist Casualty Severity

Bisikletli Yaralanma Derecesini Tahmin Etmek için Kullanılan Random Forest ve Support Vector Machine Algoritmalarının Performanslarının Test Edilmesi

Nurten AKGÜN[1]*

[1]Civil Engineering, Engineering and Natural Sciences, Bursa Technical University, Bursa, Turkey.
[1]nurten.akgun@btu.edu.tr

Received: 03.08.2023
Accepted: 26.09.2023
Revision: 10.09. 2023
doi: 10.5505/fujece.2023.57966
Research Article

Citation: Akgün N. "Testing the performance of random forest and support vector machine algorithms for predicting cyclist casualty severity". *Firat University Journal of Experimental and Computational Engineering*, 2(3), 124-133, 2023.

Abstract
Traditional statistical regression models for predicting casualty severity have fundamental limitations. Machine learning algorithms for classifications have started to be applied in severity analysis in order to relax the assumptions and provide better accuracy in the models. However, the performances of highly advised classification algorithms for predicting cyclist casualty severity, which particularly occurred at roundabouts, have not been investigated comprehensively. Therefore, the study in this paper developed classification models for cyclist casualty severity prediction by applying the highest two advised algorithms in the literature namely Random Forest and Support Vector Machine. The dataset included 439 cyclist casualties which were recorded at give-way roundabouts in the North East of England. The predictive variables were sociodemographic information about cyclists, weather conditions, behavior-related contributory factors, speed limit, and roundabout geometrical parameters. 70% of the records were randomly selected for the training stage and 30% were used for the testing in both Random Forest and Support Vector Machine algorithms. After training the algorithm, the testing results showed that the Random Forest algorithm predicted the outcomes with 88.6% classification accuracy. On the other hand, Support Vector Machine algorithm predicted the testing values with 84.73% classification accuracy. The algorithms misestimated 18 and 20 of the casualties in Random Forest and Support Vector Machine, respectively. The outcomes suggested that both Random Forest and Support Vector Machine algorithms were applicable for cyclist casualty severity prediction models with high performance.

Keywords: Machine learning, Cyclist safety, Geometry, Roundabout, Classification accuracy

Özet
Kaza yaralanma derecesinin tahmininde kullanılan geleneksel istatistiksel regresyon modellerinin birtakım kısıtlamaları vardır. Varsayımları ortadan kaldırmak ve modellerde daha iyi doğruluk sağlamak amacıyla makine öğrenmesi tekniğinin sınıflandırma algoritmaları yaralanma derecesi analizinde uygulanmaya başlanmıştır. Ancak, uygulanması tavsiye edilen sınıflandırma algoritmalarının performansları, özellikle dönel kavşaklarda meydana gelen bisikletli kazalarının yaralanma derecesini tahmin etmek için, kapsamlı bir şekilde araştırılmamıştır. Bu sebeple, bu makaledeki çalışmada, literatürde en sık önerilen iki algoritma olan Random Forest ve Support Vector Machine'i bisikletli yaralanma derecesinin tahmininde kullanarak sınıflandırma modelleri geliştirmiştir. Veri seti, İngiltere'nin kuzey-doğu bölgesinde karma kullanımlı trafiğe sahip dönel kavşaklarda meydana gelen 439 bisikletli kazalarını içermektedir. Bağımsız değişkenler bisikletlilerin sosyodemografik bilgileri, hava koşulları, sürücü davranışı ile ilgili faktörler, hız limiti ve kavşak geometrik parametreleridir. Hem Random Forest hem de Support Vector Machine algoritmalarının eğitim aşamasında veri setinin %70'i, test aşamasında ise %30'u kullanılmıştır. Algoritmaların test aşamasından sonra ortaya çıkan sonuçlara göre, Random Forest yönteminin sınıflandırma doğruluğunun %88.6 olduğu belirlenmiştir. Support Vector Machine algoritmasının ise %84.73 sınıflandırma doğruluğu ile tahmin modeli oluşturduğu tespit edilmiştir. Yanlış tahmin edilen veri sayısı Random Forest yönteminde 18 iken Suppport Vector Machine yönteminde 20'dir. Sonuçlar, hem Random Forest hem de Support Vector Machine algoritmalarının, bisikletli kaza yaralanma derecesi tahmin modelleri oluşturmak için yüksek performansa sahip uygulanabilirliklerinin olduğunu göstermektedir.

Anahtar kelimeler: Makine öğrenmesi, Bisikletli güvenliği, Geometri, Dönel kavşak, Sınıflandırma doğruluğu

*Corresponding author

1. Introduction

Give-way (non-signalized) roundabouts increase capacity [1], and delays are distributed more uniformly when traffic flows are balanced [2]. The "priority to right" give-way rule at roundabouts has been applied in the United Kingdom since 1996. Under this rule, drivers entering the roundabout must yield and give priority to circulating traffic [3]. Give-way roundabouts eliminate the number of conflict points which are potential collision locations [4]. In addition, they provide route deflection and force drivers to decrease their speed [2, 5, 6]. It was suggested that the recorded number of collisions and serious injuries for motor vehicle drivers reduced after converting signalized intersections to give-way roundabouts [7]. Therefore, there is a trend to convert signalized intersections to give-way roundabouts. However, give-way roundabouts are known to be less safe for cyclists compared to signalized intersections [8-10]. Converting signalized intersections to give-way roundabouts increases both collision number and severity [7, 11-13]. It has been suggested that approximately 25% of cyclists prefer to change their routes to avoid multilane give-way roundabouts [14] or accept the risk of casualty despite feeling unsafe [15].

Safety for cyclists at roundabouts depends on several factors, such as geometry, speed, pavement, markings, signage, driver/cyclist's age, gender, behavior, education, public awareness, and enforcement [8, 16, 17]. In particular, geometry and behavior-related contributory factors play a key role in improving safety for cyclists [18, 19]. Gaining a deeper understanding of parameters that affect cyclist crash severity at roundabouts is essential to improve safety. Prediction methods have been widely used to explore the influences on crash severities [20] and reduce the records [21]. Severity has an ordinal or binary data structure such as slight, serious and killed; therefore, logistic regression modeling approach has been applied in the majority of the former studies [1, 16, 18, 19, 22]. In addition, Poisson regression [16, 23], linear regression [9, 24] and gamma regression [23] models were applied to cyclist safety prediction research.

Traditional regression algorithms have inflexible assumptions such as linearity, independence of errors, normality, and multicollinearity [25]. The structure of the dataset collected from the real environment usually does not meet these assumptions. In addition, the number of variables in a regression model is important. Adding all variables into the regression model may cause overfitting and inefficiency. Adding a few variables may also cause underfitting and provide biased results [26]. These issues of traditional regression models reveal a significant limitation that offers a new prediction method, namely machine learning algorithms [27]. Therefore, machine learning algorithms have gained significant attention in developing accurate road crash severity prediction methods [28].

Developing crash severity prediction models using machine learning algorithms, which is a sub-division of artificial intelligence, has gained attention since 2001. The performances of different types of applied algorithms, such as Bayesian Network, K-Nearest Neighbors, Support Vector Machine, Random Forest, Multi-layer Perceptron, Artificial Neural Network, and Decision Tree, were reviewed [28]. It was suggested that Random Forest provided the highest accuracy in 70% of the applied prediction studies [28]. The second successful algorithm was Support Vector Machine and it was followed by Decision Tree and K-Nearest Neighbors. However, temporal instability was observed in the applied prediction algorithms in the literature. There is a significant need in this research field to explore the accuracy of the algorithms by using different types of casualty severity data [28]. This gap is even more significant in cyclist safety research because the majority of the studies focus on vehicle-vehicle crash records.

The number of applied cyclist casualty studies [29-35] was not sufficient in order to determine the best performance machine learning algorithms. An earlier Advanced Driver Assistance Systems based study was carried out considering vehicle cyclist realistic scenario [35]. Binary classifiers namely Support Vector Machine and Multiple Instance Learning algorithms were used to analyze 99 scenarios. The results suggested that these two algorithms were found to be applicable to detect and classify the scenarios with high accuracy. A comparison of these two algorithms suggested that Support Vector Machine gave the best performance by 87.9%. The outcomes revealed that different algorithms gave different performance levels to predict the safety for cyclists. Therefore, further studies focused on applying several classification algorithms in order to explore the best performance for prediction models.

A UK based study [33] aimed to analyze cyclist-vehicle crash severity by using Ordered Forest machine learning algorithm. Ordered Forest classifier, which was a subclass of traditional Random Forest, showed a fair performance by

approximately 50%. The outcomes suggested that cyclist/driver' behavior, age and speed limit were statistically significant in the classification model. A similar Indian dataset including 160.597 cyclist casualty severity records was analyzed using Naive Bayes, Logistic Regression, Random Forest and Decision Tree classification techniques [32]. Random Forest provided the highest accuracy by 98%. The model showed that weather and road surface conditions and speed limit were found to be significant in predicting cyclist casualty severity. A comprehensive study [34] was carried out to develop a classification model for cyclist casualty severity. The study applied several algorithms which were Logistic Regression, Gradient Boosting, Naive Bayes, Random Forest, Gaussian Naive Bayes, Ridge, Support Vector Machine, Decision Tree, Extra Tree, Linear Support Vector Machine, Perceptron Algorithm, and K-nearest Neighbors. The compared performance outcomes suggested that Extra Tree algorithm gave the best performance among the applied techniques. The statistically significant variables were noted as sociodemographic, speed limit, traffic control, road user behavior, weather, road geometry and surface condition related predictive parameters.

Not only the importance of the type of algorithm but also the sampling technique was observed. The study [31] used Decision Tree and logistic regression algorithm to explore the impacts on vulnerable road users' crash severity. The study applied different resampling techniques namely under, over and synthetic sampling. The results suggested that over sampling increased the performance of used classification algorithms. The outcomes of the prediction showed that road infrastructure and sociodemographic variables had an influence on casualty severity. A study [30] aimed to explore the performance of hybrid models. These hybrid models are a mix of Fuzzy Logit and Decision Tree algorithms, namely Decision Tree based converted Fuzzy Logit (DT-CFL) and Decision Tree based revised Fuzzy Logit (DR-RFL). The dataset considered road infrastructure, geometry, weather conditions and behavior related contributory factors as predictive variables. The outcomes suggested that gender, vehicle damage-extent, road and pavement type, and vehicle-movement were found statistically significant in both models. Regarding the algorithm comparison analysis, the performance of DT-RFL was higher than DT-CFL with 69.96 % and 59.22% accuracy levels, respectively. The other current study [29] applied Neural Network algorithm and suggested that a joint correlation analysis using machine learning techniques might be a novel approach for cyclist casualty severity studies.

The current knowledge in the literature suggests that different algorithms and sampling techniques provided different level of model performance and a solid approach for analysis of casualty severity has not been determined yet. The second important gap in the literature was the target groups in the data. The majority of the studies analyzed either vehicle-vehicle or motorcyclist-vehicle crash severities. However, vulnerable road user crash severities, particularly cyclists, have not been analyzed comprehensively. A third significant gap in the literature was none of the studies focused on intersections, particularly give-way roundabouts as known dangerous for cyclists. Considering these gaps, the research in this paper aimed to apply the two highest recommended machine learning algorithms, Random Forest and Support Vector Machine, to explore the impact on cyclist casualty severity that occurred at give-way roundabouts with mixed traffic.

Machine learning algorithm has a learning process from a set of data and develops a classification or prediction model [36]. The advantage of machine learning is making no assumption about the structure or relationship between the predictive variables. Therefore, it is more preferable than traditional statistical techniques [34]. It has three types of learning supervised, unsupervised and semi-supervised [27]. Both of the algorithms used in this research, Random Forest and Support Vector Machine, are supervised classification techniques. Random Forest is developed from decision tree technique that creates a forest (Figure 1). The input values create the trees in the forest and the output shows the accuracy of the model. The higher number of variables in the model increases the accuracy of the algorithm [32]. Random Forest is a subdivision of Decision Tree method but the knowledge in the literature suggests that Random Forest gives better performance than Decision Tree technique [37]. Support Vector Machine is a type of supervised learning binary model [35]. The algorithm segregates and classifies the input and builds a hyperplane to separate the classes [38]. Support vectors are the points that are close to the dividing line and the margin is the distance between support vectors and the dividing line [39]. These two algorithms were widely applied in modeling crashes by severity because severity has bivariate (non-injured, injured) or multivariate (slight, serious, killed) levels [27]. Random Forest outperformed Decision Tree in the research conducted by [40, 41]. Despite the applied alternative methods such as K-Nearest Neighbor and Support Vector Machine in these studies, RF consistently demonstrated superior performance.

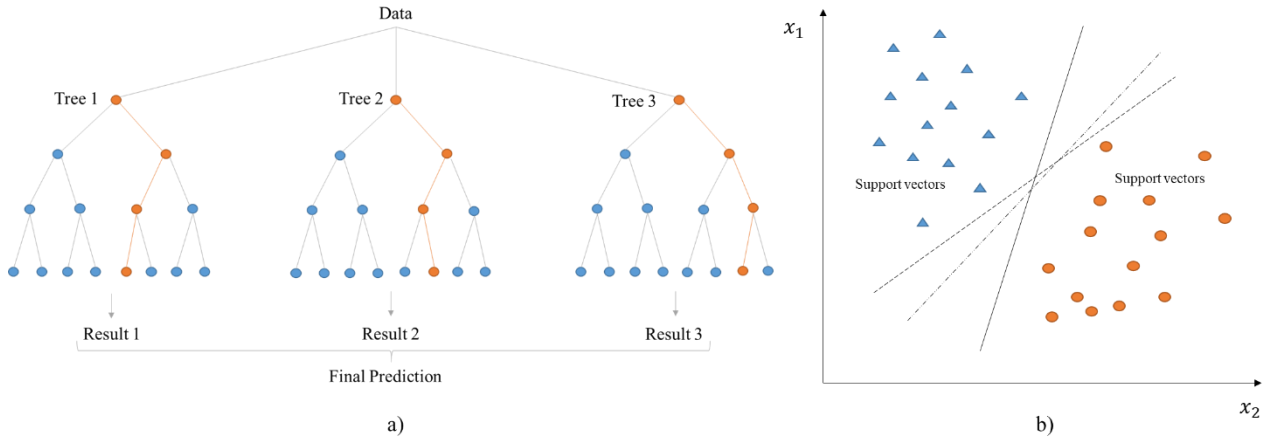

Figure 1. a) Random Forest algorithm, trees in a forest; b) Support Vector Machine algorithm, possible separating hyperplanes

The objectives of the research are to develop a cyclist casualty prediction model and compare the performance of applied algorithms in order to contribute to the gap in the literature. Section 2 explains the methodology of the research and the structure of the data. The results are presented in Section 3. Finally, discussion, recommendations and limitations are given in Section 4.

2. Methodology

The supervised classification technique was selected to apply because the response variable of the dataset was categorical values as casualty severity (slight and serious). The records did not have killed casualties; therefore, the response values were binary classes. Random Forest and Support Vector Machine algorithms were applied using the same dataset and the obtained classification accuracies from both methods were compared. Classification accuracy is calculated using a confusion matrix. The outcome variable has binary values such as slight and serious; therefore, the confusion matrix has two categories with a 2x2 matrix. There are four predicted options on the matrix which are True Positives: slight is predicted and the real output is slight, True Negatives: serious is predicted and the real output is serious, False Positives: slight is predicted and the real output is serious, False Negatives: serious is predicted and the real output is slight. False Positive is type 1 error and False Negative is type 2 error. Classification accuracy is the ratio of the correct number of predictions to the total number of predictions across all three classes. The accuracy ranges between 0-1 and it should be as high as possible. The overall accuracy can be calculated as given in Equation 1 [34].

$$Classification\ Accuracy\ =\ (True\ Positive\ +\ True\ Negative)\ /\ Total\ Sample \tag{1}$$

The Northumbria region located in the North East of England was chosen as a case study (See Figure 2). In the case study area, cyclists have to share the road with private motor vehicles due to the lack of cycling infrastructure facilities. The cyclist casualty at give-way roundabout data from the UK STATS19 police records was provided through the Traffic and Accident Data Unit which is held by Gateshead Council. In the study area, comprehensive collision records have been collected by the local authorities since 2010; therefore, the data for the period of 2011-2016 were analyzed in this work. The data includes geographical coordinates of the roundabouts where the collision occurred. The physical data for the roundabouts where the collisions occurred was obtained as maps from Digimap in the form of AutoCAD files, and the geometric variables and coordinates of collisions were imported to these maps. Roundabout geometric design variables were determined by considering the regulations given in the UK road design manual (Figure 2) [42]. The dataset included 370 slight and 69 serious cyclist casualty records. There was no missing value in the dataset. The predictor variables were cyclist's gender and age, light, weather and road surface conditions, speed limit, and behavior related to contributory factors such as failed to look properly, careless, passing closed to cyclist, failed to judge other person's path or speed, and poor turn or maneuver. Data also included roundabout geometric design variables namely approach number of lanes, approach width, entry path radius, number of arms, inner circle radius, entry width, entry number of lanes, and circulating number of lanes. The descriptive statistics, Random Forest and Support Vector Machine algorithms were applied in the R statistical analysis program.

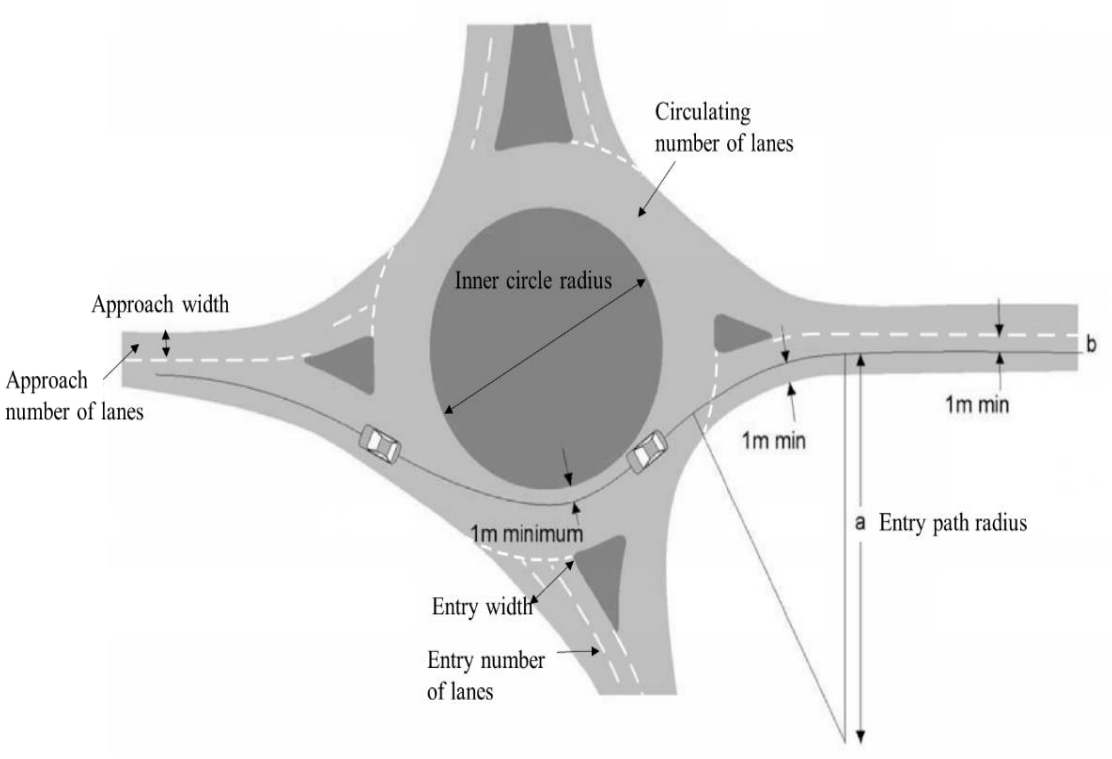

Figure 2. Roundabout geometric design parameters [42].

3. Results

Descriptive statistic was applied and the results showed that the number of male cyclists was higher than females (Table 1). As stated in the state of the art review, cyclists avoided using roundabouts with mixed traffic [14]. This situation might be even more significant considering the gender. In addition, the unpopularity of cycling among females might reduce the number of female cyclists and therefore the number of female records might be significantly less than males. The mean age was 39 for slight and 41 for serious casualties. This might be the higher cycling rates for middle age male road users. The majority of the casualties occurred in daylight, fine weather and dry road surface conditions. It should be noted that cyclists might not prefer cycling under heavy environmental conditions. Approximately 80% of the casualties had failed to look properly issue at roundabouts. This is followed by not judging other road user's path by %23. The majority of the records were observed at roundabouts with a 30mph speed limit and four arms due to the high rate of urban cycling demand.

Table 1. Descriptive statistics of variables

Variable	Slight Casualty	Serious Casualty
Gender	Female (45); Male (325)	Female (10); Male (59)
Age	Min. (5); Max. (77); Mean (39); S.D. (14)	Min. (15); Max. (80); Mean (41); S.D. (14)
Light condition	Darkness (83); Daylight (287)	Darkness (15); Daylight (54)
Weather	Fine (313); Rain (45); Other (12)	Fine (60); Rain (9); Other (0)
Road surface	Dry (261); Wet (100); Ice (9)	Dry (51); Wet (18); Ice (0)
Failed to look properly	Yes (291); No (79)	Yes (58); No (11)
Careless	Yes (85); No (285)	Yes (14); No (55)
Passing too closed to cyclist	Yes (49); No (321)	Yes (9); No (60)
Failed to judge other person's path or speed	Yes (91); No (279)	Yes (10); No (59)
Poor turn or maneuver	Yes (45); No (325)	Yes (6); No (63)
Speed limit (mph)	20 (3); 30 (280); 40 (33); 50 (12); 60 (33); 70 (9)	20 (2); 30 (43); 40 (8); 50 (1); 60 (9); 70 (6)
Approach number of lanes	1 (274); 2 (90); 3 (6)	1 (32); 2 (36); 3 (1)
Approach width (meter)	Min. (3); Max. (11.37); Mean (5.15); S.D. (1.79)	Min. (3); Max. (8.78); Mean (5.81); S.D. (1.66)
Entry path radius (meter)	Min. (19.23); Max. (99.83); Mean (64.36); S.D. (20.58)	Min. (23.77); Max. (99.98); Mean (80.74); S.D. (20.35)
Arms (3; 4; 5; 6)	3 (60); 4 (245); 5 (53); 6 (12)	3 (13); 4 (41); 5 (12); 6 (4)
Inner circle radius (meter)	Min. (1.00); Max. (124.79); Mean (18.36); S.D. (23.06)	Min. (1.00); Max. (124.79); Mean (20.01); S.D. (23.71)
Entry width (meter)	Min. (3.00); Max. (20.27); Mean (7.68); S.D. (2.60)	Min. (4.00); Max. (12.66); Mean (7.87); S.D. (2.26)
Entry number of lanes	1 (168); 2 (180); 3 (22)	1 (21); 2 (41); 3 (6); 4 (1)
Circulating number of lanes (1; 2; 3)	1 (237); 2 (127); 3 (6)	1 (33); 2 (35); 3 (1)

It is suggested in the literature that, approximately 60-80% of the data is used for training and the rest of the data is used for testing. More in detail, the majority of the crash severity analysis used 70% for training and 30% for testing [27]. With respect to the applied casualty severity studies in literature, in the Random Forest algorithm, 70% of the data were randomly selected for the training stage and 30% was used for the testing. All the predictive variables were used in the algorithm. After training the algorithm, the testing procedure started and the results showed that the Random forest algorithm predicted the outcomes with 88.6% of classification accuracy. In the Support Vector Machine algorithm, 70 % of the data were used for the training and 30 were used for the tasting stages. The results showed that the model predicted the testing values with 84.73% classification accuracy. It only misestimated 18 and 20 of the casualties in Random Forest and Support Vector Machine algorithms, respectively (Table 2).

Table 2. Random Forest and Support Vector Machine outcomes

Algorithm	Testing Outcomes (Confusion Matrix)			Classification Accuracy
Random Forest		Slight	Serious	88.60%
	Slight	136	3*	
	Serious	15**	4	
Support Vector Machine		Slight	Serious	84.73%
	Slight	111	20*	
	Serious	0**	0	

*Type 1 Error
**Type II Error

An example tree of the Random Forest is given in Figure 3. It can be seen that the root of the tree started with the approach number of lanes. If the lane number was 1, the branch grew in the left direction; and if no, in the right direction. The

Random Forest algorithm created several trees which generated a forest. The average results of these forests provided a final prediction. Regarding the Support Vector Machine algorithm, the hyperplane was not drowned because the model was multi-dimensional. It was aimed to improve the performance of the Support Vector Machine and the C parameters were customized in classification. Different C parameters (i.e. 0, 0.01, 0.05, 0.1, 0.25, 0.5, 0.75, 1, 1.25, 1.5, 1.75, and 2.5) were coded in the algorithm. The model was trained with the new C parameters and the testing was carried out. The higher C parameter reduced the accuracy of the model (Figure 4). This result was expected because a larger C parameter considers the outliers while creating a hyperplane. Hyperplane should separate the values correctly and the margin should be minimum. However, both cases may not occur at the same time. When the C parameter is low, the hyperplane is located with a large minimum margin but some outliers can be observed. Therefore, a higher C parameter may change the location of the hyperplane and the accuracy of the model can be affected. In this analysis, the increase in the C parameter reduced the classification accuracy.

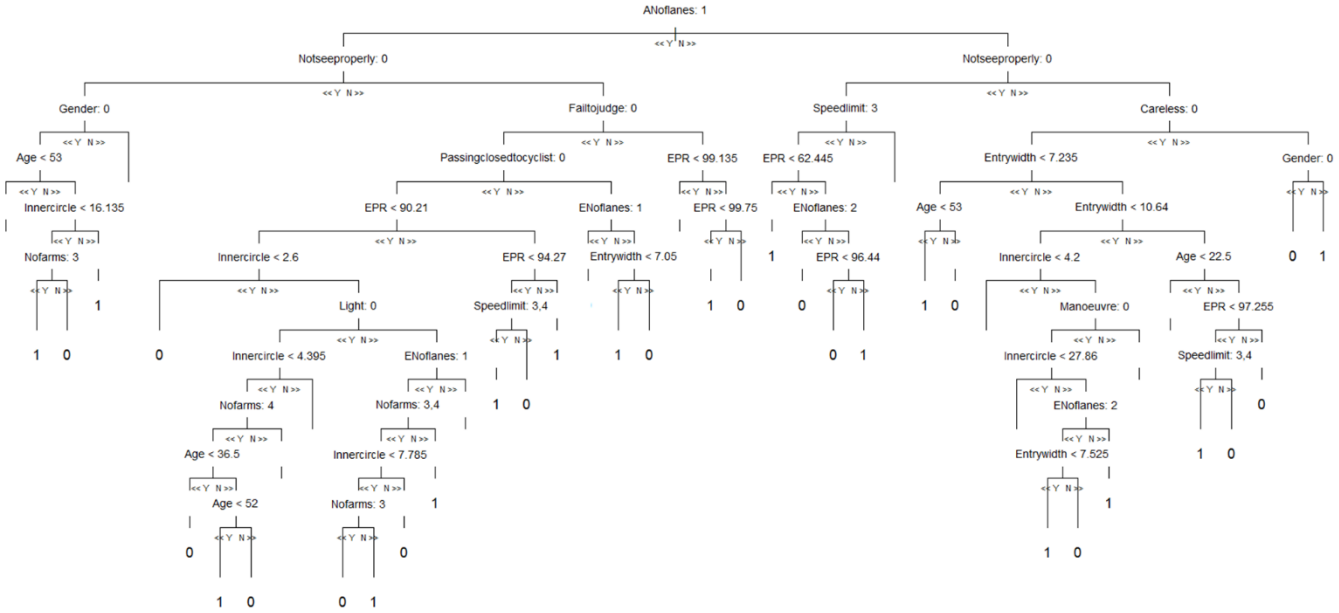

Figure 3. Accuracy outcomes for different C parameters

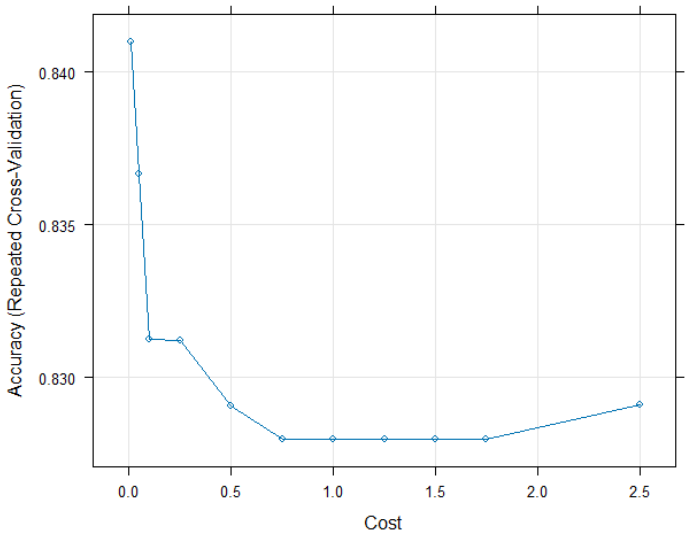

Figure 4. Accuracy outcomes for different C parameters

4. Discussion

The study in this paper explored the performance of Random Forest and Support Vector Machine algorithms to predict cyclist casualty severities. The results suggested that Random Forest performed slightly better than Support Vector Machine. This outcome was expected since the majority of the studies in the literature suggested that Random Forest was the top recommended algorithm with the highest accuracy among the other machine learning algorithms [28]. However, further studies should consider other types of algorithms. For instance, research suggested [34] that Extra Tree algorithm performed better than Random Forest. It is clearly seen that Random Forest has been the most advised algorithm but the results might change for every dataset.

The outcomes of this paper showed that the classification accuracy was 88.6% for the Random Forest algorithm. However, the former study which applied Random Forest reached higher accuracy with 98% [32]. This study [32] and the research in this paper used a similar dataset structure; however, the number of sample size was 160.597 in the former study [32]. This suggests that increasing the sample size can increase the classification accuracy of the algorithm. A similar conclusion was observed for Support Vector Machine algorithm. The results in this analysis suggested that classification accuracy was 84.73%; while a previous study reached 87.9% [35]. However, the study in this paper suggests that high accuracy can be obtained with 439 casualty records. It should be noted here that the number of variables used in the algorithm is also important because more variables in the model increase the accuracy of the machine learning algorithms [32].

Considering the given knowledge in the literature [27], the majority of the former studies used 70% of the data for training and 30% for testing in the analysis. This study in this paper also used a 70/30 ratio in both algorithms. However, the 70/30 ratio is a rule of thumb and it can be extended from 60/40 to 80/20. Future studies can consider different types of ratios in the analysis. In addition, a comparative study can be conducted considering different ratios for different classification algorithms.

The limitation of this study was the limited number of casualty records. Future studies may consider applying Random Forest and Support Vector Machines classifiers using around 440 observations; however, increasing the sample size is suggested. Furthermore, machine learning algorithms are still in development process. Some derivative algorithms, such as Ordered Forest [33], can be considered in further research.

5. Acknowledgement

The casualty severity data was obtained from Gateshead Council, England.

6. Author Contribution Statement

In the study, Author 1 contributed to literature review, methodology, analysis and writing up the article.

7. Ethics Committee Approval and Conflict of Interest

Ethics committee approval is not needed for preparing the article.
There is no conflict of interest for this article.

8. References

[1] Silvano AP, Ma X, Koutsopoulos HN. "When do drivers yield to cyclists at unsignalized roundabouts". *Transportation Research Record: Journal of the Transportation Research Board*, 2520, 2015.
[2] Silvano AP, Linder, A. "Traffic safety for cyclists in roundabouts: Geometry, traffic, and priority rules". *Swedish National Road and Transport Research Institute*, 2017.
[3] Bruce W, Rodegerdts L, Scarborough W, Kittelson W, Troutbeck R, Brilon W, Bondzio L, Courage K, Kyte M, Mason J, Flannery A, Myers E, Bunker J, Jacquemart G. "Roundabouts: an informational guide". US Department of Transport: Federal Highway Administration, AASHTO, 2000.
[4] Poudel N, Singleton PA. "Bicycle safety at roundabouts: a systematic literature review". *Transport Reviews*, 41 (5), 617-642, 2021.
[5] Retting RA, Persaud BN, Garder PE, Lord D. "Crash and injury reduction following 17 installation of roundabouts in the United States". *American Journal of Public Health*, 91 (4), 628-31, 2001.
[6] Gross F, Lyon C, Persaud B, Srinivasan R. "Safety effectiveness of converting signalized intersections to roundabouts*". Accident Analysis & Prevention*, 50, 234–241, 2013.
[7] De Brabander B, Vereeck L. "Safety effects of roundabouts in Flanders: signal type, speed limits and vulnerable road users". *Accident Analysis & Prevention*, 39 (3), 591-599, 2007.
[8] Furtado G. "Accommodating vulnerable road users in roundabout design". Annual Conference of the Transportation, Canada, Quebec City, 2004.
[9] Daniels S, Brijs T, Nuyts E, Wets G. "Injury crashes with bicyclists at roundabouts: influence of some location characteristics and the design of cycle facilities". *Journal of Safety Research*, 40 (2), 141-148, 2009.
[10] Jensen SU. "Safe roundabouts for cyclists". *Accident Analysis & Prevention*, 105, 30-37, 2017.
[11] Robinson BW, Rodegerdts L, Scarborough W, Kittelson W, Troutbeck R, Brilon W, Bondzio L, Courage K, Kyte M, Mason J, Flannery A, Myers E, Bunker J, Jacquemart G. "Roundabouts: an informational guide". FHWA-RD-00-067, Project 2425, Informational Guide Book, 2000.
[12] Persaud BN, Retting RA, Garder PE, Lord D. "Observational before-after study of the safety effect of U.S. roundabout conversions using the empirical Bayes method". *Annual Meeting of the Transportation Research Board*, TRB ID: 01-0562, 2001.
[13] Elvik R. "Effects on road safety of converting intersections to roundabouts: review of evidence from non-US studies". *Transportation Research Record: Journal of the Transportation Research Board*, 1847 (1), 2003.
[14] Arnold LS, Flannery A, Ledbetter L, Bills T, Jones MG, Ragland DR, Spautz L. "Identifying factors that determine bicyclist and pedestrian: involved collision rates and bicyclist and pedestrian demand at multi-lane roundabouts". UC Berkeley Safe Transportation Research & Education Center, I.o.T.S. University of California, Berkeley, 2010.
[15] Davies DG, Taylor MC, Ryley TJ, Halliday ME. "Cyclists at roundabouts — the effects of 'Continental' design on predicted safety and capacity". *Transport Research Laboratory*, 1997.
[16] Hels T, Orozova-Bekkevold I. "The effect of roundabout design features on cyclist accident rate". *Accident Analysis & Prevention*, 39 (2), 300-307, 2007.
[17] Montella A. "Identifying crash contributory factors at urban roundabouts and using association rules to explore their relationships to different crash types". *Accident Analysis & Prevention*, 43 (4), 1451-1463, 2011.
[18] Akgün N, Dissanayake D, Thorpe N, Bell MC. "Cyclist casualty severity at roundabouts – To what extent do the geometric characteristics of roundabouts play a part?". *Journal of Safety Research*, 67, 83–91, 2018.
[19] Akgün N, Daniels S, Bell MC, Nuyttens N, Thorpe N, Dissanayake D. "Exploring regional differences in cyclist safety at roundabouts: A comparative study between the UK (based on Northumbria data) and Belgium". *Accident Analysis & Prevention*, 150, 105902, 2021.
[20] Wang C, Quddus MA, Ison SG. "Predicting crash frequency at their severity levels and its application in site ranking using a two-stage mixed multivariate model". *Accident Analysis & Prevention*, 43 (6) (2011), 1979-1990, 2011.
[21] Savolainen P, Mannering F, Lord D, Quddus MA. "The statistical analysis of crash-injury severities: a review and assessment of methodological alternatives". *Accident Analysis & Prevention*, 43 (5) (2011), 1666-1676, 2011.
[22] Daniels S, Brijs T, Nuyts E, Wets G. "Externality of risk and crash severity at roundabouts". *Accident Analysis & Prevention*, 42 (6), 1966-1973, 2010.
[23] Daniels S, Brijs T, Nuyts E, Wets G. "Extended prediction models for crashes at roundabouts". *Safety Science*, 49 (2), 198-207, 2011.

[24] Møller M, Hels T. "Cyclists' perception of risk in roundabouts". *Accident Analysis & Prevention*, 40 (3), 1055-1062, 2008.
[25] Field A. Discovering Statistics Using SPSS. 3rd Edition, SAGE Publications Ltd, 2009.
[26] Peduzzi P, Concato J, Kemper E, Holford TR, Feinstein AR. "A simulation study of the number of events per variable in logistic regression analysis". *Journal of Clinical Epidemiology*, 49 (12), 1373-1379, 1996.
[27] Silva PB, Andrade M, Ferreira S. "Machine learning applied to road safety modeling: A systematic literature review". *Journal of Traffic and Transportation Engineering* (English Edition), 7 (6), 775-790, 2020.
[28] Santos K, Dias JP, Amado C. "A literature review of machine learning algorithms for crash injury severity prediction". *Journal of Safety Research*, 80, 254-269, 2022.
[29] Janstrup KH, Kostic B, Møller M, Rodrigues F, Borysov S, Pereira FC. "Predicting injury-severity for cyclist crashes using natural language processing and neural network modelling". *Safety Science*, 164, 106153, 2023.
[30] Katanalp BY, Eren E. "The novel approaches to classify cyclist accident injury-severity: Hybrid fuzzy decision mechanisms". *Accident Analysis & Prevention*, 144, 105590, 2020.
[31] Vilaça M, Macedo E, Coelho MC. "A Rare event modelling approach to assess injury severity risk of vulnerable road users". Safety, 5(2), 29, 2019.
[32] Yamparala R, Challa R, Valeti P, Chaitanya PS. "Prediction of cyclist road accidents in india using machine learning and visualization techniques". Second International Conference on Artificial Intelligence and Smart Energy (ICAIS), Coimbatore, India, 476-481, 2022.
[33] Zhang Y, Li H, Ren G. "Analyzing the injury severity in single-bicycle crashes: An application of the ordered forest with some practical guidance". *Accident Analysis & Prevention*, 189, 107126, 2023.
[34] Birfir S, Elalouf A, Rosenbloom T. "Building machine-learning models for reducing the severity of bicyclist road traffic injuries". *Transportation Engineering*, 12, 100179, 2023.
[35] Cara I, De Gelder E. "Classification for safety-critical car-cyclist scenarios using machine learning". IEEE 18th International Conference on Intelligent Transportation Systems, Gran Canaria, Spain, 1995-2000, 2015.
[36] Fan J, Ma C, Zhong Y. "A selective overview of deep learning". Statistical Science, 36(2), 264-290, 2021.
[37] Li L, Shrestha S, Hu G. "Analysis of road traffic fatal accidents using data mining techniques". Ieee 15th International Conference on Software Engineering Research, Management and Applications (Sera), 363–70, 2021.
[38] Boser BE, Guyon IM, Vapnik VN. "A training algorithm for optimal margin classifiers". Proceedings of the 5th Annual Workshop on Computational Learning Theory, 144-152, 1992.
[39] Suthaharan S. "Support vector machine - In Machine learning models and algorithms for big data classification". Integrated Series in Information Systems, 207–235, Springer, 2016.
[40] Wahab L. Jiang H. "A comparative study on machine learning based algorithms for prediction of motorcycle crash severity". PLoS one, 14-4, 2019.
[41] Zhang J, Li Z, Pu Z, Xu C. "Comparing Prediction Performance for Crash Injury Severity Among Various Machine Learning and Statistical Methods". IEEE Access, 6, 60079-60087, 2018.
[42] DfT. "TD 16-07 Geometric design of roundabouts". Department for Transport, the UK, 2007.

Firat Univ Jour. of Exp. and Comp. Eng., 2(3), 134-148, 2023

Firat University Journal of Experimental and Computational Engineering
Fırat Üniversitesi Deneysel ve Hesaplamalı Mühendislik Dergisi

An Ultraviolet Germicidal Irradiation Autonomous Robot

Bir Ultraviyole Antiseptik Işınlama Otonom Robotu

Augustus Ehiremen Ibhaze[1]*, Favour Moyosoreoluwa Adekogbe[2]

[1,2]Department of Electrical and Electronics Engineering, Faculty of Engineering, University of Lagos, Akoka, Lagos, Nigeria
[1]eibhaze@unilag.edu.ng, [2]favouradekogbe@gmail.com

Received: 28.07.2023
Accepted: 06. 10. 2023
Revision: 12.09.2023
doi: 10.5505/fujece.2023.83703
Research Article

Citation: Ibhaze AE, Adekogbe FM. "An ultraviolet germicidal irradiation autonomous robot". *Firat University Journal of Experimental and Computational Engineering*, 2(3), 134-148, 2023.

Abstract

Utilization of UV light for disinfection and sterilization has increased as a result of its germicidal properties; nevertheless, due to its adverse effects on the skin and eyes, this poses a risk to individuals. The demand for autonomous UV robots originates from the requirement that UV disinfection must occur without human intervention in order to minimize health risks and take advantage of UV light as a disinfection mechanism. This study focuses on the development of a UV disinfection robot that navigates autonomously via obstacle detection and avoidance using Raspberry Pi 4 model B interfaced with UV light and YOLOv4 for high touch object detection. The UV disinfection robot uses object detection to find objects that come into touch with hands frequently and successfully cleans them with UV light. The robot uses an embedded system with a Raspberry-Pi controller, motion sensors, and detects human presence because UV radiation may be harmful to humans. Without human intervention, the autonomous UV disinfection system was effective in cleaning surfaces. Based on the findings in this study, the dosimeter showed a very faint purple tint at 10, 20, and 30 minutes that ranges from 0 to 25 mJ/cm^2. Between 45 and 60 minutes, and between 25 and 50 mJ/cm^2, the dosimeter exhibited a vivid purple color. These results showed that even though different bacteria require different exposure durations to become inactive, a minimum disinfection time of 10 minutes is required to conduct any type of disinfection.

Keywords: Autonomous robot, Convolutional network, Germicidal irradiation, LED, Ultraviolet light

Özet

UV ışığının antiseptik özelliklerinin bir sonucu olarak dezenfeksiyon ve sterilizasyon amacıyla kullanımı artmıştır; ancak cilt ve gözler üzerindeki olumsuz etkileri nedeniyle bireyler için risk oluşturmaktadır. Otonom UV robotlarına olan talep, sağlık risklerini en aza indirmek ve bir dezenfeksiyon mekanizması olarak UV ışığından yararlanmak için UV dezenfeksiyonunun insan müdahalesi olmadan gerçekleşmesi gerekliliğinden kaynaklanmaktadır. Bu çalışma, yüksek temaslı nesne tespiti için UV ışığı ve YOLOv4 ile ara yüzlenen Raspberry Pi 4 model B'yi kullanarak engel tespiti ve kaçınma yoluyla otonom olarak hareket eden bir UV dezenfeksiyon robotunun geliştirilmesine odaklanmaktadır. UV dezenfeksiyon robotu, ellerle sık temas eden nesneleri bulmak için nesne algılamayı kullanır ve bunları UV ışığıyla başarılı bir şekilde temizler. Robot, Raspberry-Pi denetleyicisi ve hareket sensörleri içeren gömülü bir sistem kullanıyor ve UV radyasyonu insanlara zararlı olabileceğinden insan varlığını tespit ediyor. Otonom UV dezenfeksiyon sistemi, insan müdahalesi olmadan yüzeylerin temizlenmesinde etkili oldu. Bu çalışmadaki bulgulara göre dozimetre, 10, 20 ve 30. dakikada 0 ile 25 mJ/cm^2 arasında değişen çok soluk bir mor renk tonu gösterdi. 45 ile 60 dakika arasında ve 25 ila 50 mJ/cm^2 arasında dozimetre canlı mor renk sergiledi. Bu sonuçlar, farklı bakterilerin inaktif hale gelmeleri için farklı maruz kalma sürelerine ihtiyaç duymalarına rağmen, herhangi bir dezenfeksiyon türünün gerçekleştirilmesi için minimum 10 dakikalık bir dezenfeksiyon süresinin gerekli olduğunu gösterdi.

Anahtar kelimeler: Otonom robot, Evrişimli ağ, Antiseptik ışınlama, LED, Ultraviyole ışık

*Corresponding author

Plagiarism Checks: Yes – Turnitin
Complaints: fujece@firat.edu.tr

1. Introduction

The quest for proper hygiene has piqued global interest since the last global public health emergency occasioned by the COVID – 19 pandemic [1]

Effective measures to maintain hygiene while disinfecting contaminable surfaces has ever since attracted enormous research attention [2] [3] [4]. According to [5], to prevent the transmission of diseases, pathogens, such as bacteria, prions, viruses, fungus and other microbes could be removed, destroyed or rendered inactive by the decontamination procedure. This procedure is usually categorized as cleaning, sterilization and disinfection [6]. It is to be noted that both sterilization and disinfection may be carried out by utilizing UV Radiation among other methods, while cleaning requires vacuuming, mopping or scrubbing [6] [7].

Because viruses can spread through the air or by direct contact, the risk of disease transmission rises when surfaces are contaminated. To reduce the probability of disease transmission, it is pertinent to carry out proper routine disinfection of surfaces. This plays an important part in the prevention of disease transmission and ensures healthier living. This study explores the use of one of the most effective methods of disinfection and sterilization; Ultraviolet Germicidal Irradiation (UVGI) [8]. UV light, which was discovered in 1801, was used to treat and sterilize water before it was used as a disinfection method [9]. After the end of World War II in 1945, germicidal UV lamps were made commercially available and utilized to disinfect the air [9].

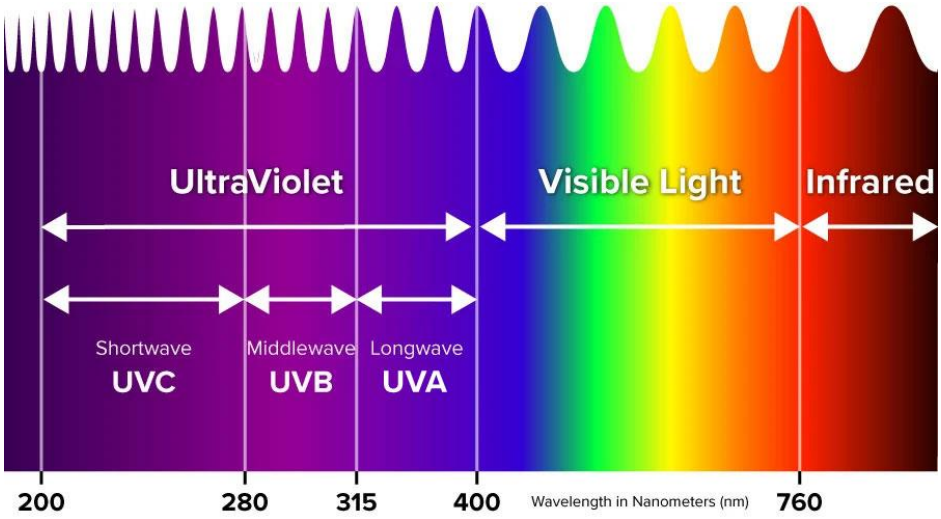

Figure 1. A section of the electromagnetic wave spectrum [10]

As shown in Figure 1, three sections of UV light are identified on the spectrum: UV-A, with a spectrum of 315–400 nm, UV-B, with a spectrum of 280–315 nm, and UV-C, with a spectrum of 200–280 nm [10] [11]. Out of these, UV-C light has the shortest wavelength (200 to 280 nanometers) and possesses the highest energy. This gives it the ability to eliminate viruses and bacteria, otherwise known as pathogens [8]. UV-C disinfects by breaking up the covalent bonds that hold the DNA of pathogens together, and 'super bugs' that have developed a very strong resistance to antibiotics are not exempt. It is effective against new viral and bacterial strains and it also eliminates the need for toxic chemicals [12].

UV-C light has been instrumental in the sterilization of surgical tools, medical equipment, and hospital rooms. It was found in a study that analyzed 21,000 patients that when combined with traditional cleaning methods, UV light disinfection resulted in a 30% reduction in the transmission of drug-resistant bacteria [12]. UV light disinfection has been deployed as fixed or mobile systems such as wands, boxes, and bottles, but this has certain limitations [8]. The fixed systems are bulky and this makes the navigation of crowded spaces difficult. It is also difficult to reach corners and shadowed areas. In the case of mobile systems, disinfection of a large area may require multiple mobile units; whereas a single unit may require more time to disinfect. The need for human control of the mobile unit is another limitation as this may result in increased cost of hiring operation personnel. Another major problem is the health hazard it presents. Human exposure to UV light

has been linked to several diseases as it penetrates the outermost layer of the skin. This leads to cell and tissue damage that could predispose to skin cancer and cataracts. It could also negatively affect the immune system.

According to the work done in [13], it was noted that before the COVID-19 pandemic, businesses and research facilities were developing disinfection robots to improve cleaning and sterilization in areas with a high risk of infection. However, in response to the pandemic, various robotic disinfection systems had been implemented. Some designs are simple combinations of commercial mobile devices with specialized UV lamps, while others are more sophisticated robotic systems that could turn UVC lamps on and off while moving through a facility [14]. For instance, AVA robotics built a movable base for MIT's UV robot that incorporates a controller for the UV light. This UV robot was utilized in food pantries. This robot utilized four UVC lamps and could cover 370 square meters in 30 minutes at a speed of 0.1m/s [15]. Another example is the Building Momentum's UVC robot 2.0, which had a mobile base with UVC lamps on top and utilized six lamps operating at 330 W with a wavelength of 254 nm for disinfection. This robot could navigate using the line-following technique [16] [17].

In the work of [18], Akara Robotics developed Violet, a UV disinfection robot that could detect humans and turn off its mercury UV lamp when humans were present. Violet had a small form factor and could navigate through tight spaces, making it suitable for use in cluttered areas such as hospital rooms with multiple medical devices [19]. To enhance its safety around humans, Violet adopted a reflective shield made of aluminum metal, which enhanced the radiation intensity [18]. It has been demonstrated that the pulsed xenon UV light used by Xenex's Lightstrike robot reduces SARS-CoV-2 on hard surfaces and face respirators [20]. The robot's wide-spectrum UV light was highly toxic to microbes and had a peak power 4300 times greater than a mercury lamp. Xenex's robot had fast disinfection cycles and could disinfect a hospital ward in 10 minutes and an operating theater in about 20 minutes [17].

The UVD Robot was created by Blue Ocean Robotics, a Danish business that specialized in creating robots for cleaning hospitals, trains, and airlines. This robot use 3D sensors to survey the environment, identify barriers, and carry out an algorithm that turns off the UV light when it detects humans or when it approaches an object too closely [17]. Medical facilities in Croatia and Romania have started using Blue Ocean Robotics' autonomous disinfection robots. The UVD robot designed using low pressure mercury (LMP) lamps could disinfect rooms in just 10 minutes [13].

The AIDBOT, developed by Dr. KangGeon Kim of the Artificial Intelligence and Robotics Institute at KIST, is a disinfection robot powered by artificial intelligence. The AIDBOT could independently navigate and disinfect a contaminated room using both disinfectants and UV light simultaneously. The ADIBOT-A, developed by UBTECH, is an autonomous UV robot that combines UVC technology with UBTECH’s expertise in robotics to create an intelligent UV disinfection system. The robot operates at a UV wavelength of 253.7 nm and could move around medical facilities autonomously. The ADIBOT-A is re-configurable, meaning it is able to modify its UVC power and height for different disinfection applications [21].

Some disinfection robots that are not completely autonomous also utilizes UVC technology. GermFalcon, a UVC airplane disinfection system, requires a human operator for it to be moved into the airplane. The robot protects its operator from UV exposure with its in-built shield [22]. A UVC robot created by Tru D Smart was deployed in a hospital for acute care, and it was able to significantly decrease pathogens like Acinetobacter in rooms of infected patients [15]. Sterilray has begun advertisement for its autonomous disinfection robot that employs excimer lamps producing far-UVC that is set to launch in 2023 [13]. Developed for the sterilization of patients or operating rooms, the UV bot by [23], utilizes three 19.3W UVC lamps, installed on top of a mobile robot base. This robot navigates with the aid of a wireless remote-control technology operated by a human operator [23]. A comparison of UV disinfection robots is depicted in Table 1.

Table 1. Comparison of UV Disinfection Robots (existing and open to research)

Robot/Properties	Autonomous	Cost (USD)	Human safety	UV Source
Aitheon's UVD Robots	Yes	-	No	LPM
Ava Robotics UV Disinfection robot	Yes	-	No	-
BlueBotics's mini UVC	Yes	-	No	-
Blue-Ocean UVD Robot	Yes	90,000	No	LPM
BooCax UV1500	Yes	-	No	Quartz lamp
GlobalDWS's DSR	Yes	-	No	-
Helios UVC System	No	125000	No	Amalgum UVC lamp
Hero21	Yes	-	No	-
Honeywell's UV System	Yes	-	No	LPM
Lumnicleanse's UVC robot	Yes	-	No	-
Prescientx's Violet	Yes	-	Yes	-
Pudu's Puductor 2	Yes	-	No	-
RoverUV	Yes	89,000	No	-
R-Zero Arc	No	-	No	-
Sterilray Far-UV Robot	Yes	90,000	No	LPM
The Badger UV Disinfect Robot	Yes	-	No	LPM
TMiRob's Intelligent Disinfection Robot	Yes	-	No	-
Tru D	No	125000	No	LPM
Violet by Akara Robotics	Yes	-	Yes	Mercury vapor UV lamp
Xenex Lightstrike	No	125,000	No	PXL
ADAMMS UV Robot	No	-	No	LPM and UV Wand
Fetch UV Robot	No	-	No	UV Flashlight
Ultrabot	No	-	Yes	LPM
G-Robot	No	-	Yes	Far-UVC

Data from: [13], [17], [18], and [24].

Table 1 compares UV robots that are existing and still under research based on their cost, autonomous ability, and human safety and UV light sources. By comparing these factors, the essential features of a UV robot could be identified and the areas that requires further research may be determined. In this study, an autonomous UV disinfection system was developed using embedded technology. This was achieved by programming the Raspberry Pi interfaced with the UV light source. To achieve the high touch object detection, You Only Look Once (YOLOv4) machine learning model was programmed to run on the Raspberry Pi microprocessor. The safety mechanism was factored into the design by using an aluminum foil as the lining behind the UV light source. This was to shield the area behind the disinfection system from the effect of the UV light and its reflecting incident light. Hence, simultaneous manual cleaning and UV disinfection could be achieved. To add built-in autonomous navigation capability into the design, the Raspberry Pi was interfaced with a proximity sensor and a motor driver.

2. Materials and Method

A microprocessor, the Raspberry Pi 4 model B, sits at the heart of the autonomous UV disinfection robot. The experimental setup as shown in Figure 2 details the implementation of the autonomous UV disinfection robot. The web camera feeds data into the microprocessor which processes this input and runs it through an object detection model for identifying high-touch surfaces such as door knobs or handles. This object detection model is based on the YOLOv4 architecture, known for the balance it offers between speed and accuracy, to ensure a high degree of precision [25]. Architecture-wise, YOLOv4 is a fully convolutional network. There are 110 convolutional layers in all. 44 of them are 3 x 3 and 66 are 1 x 1, respectively. A 3 x 3 convolution layer with 32 filters is present in the input layer. The output layer is a convolution layer with a size of 1 x 1, stride, and padding. The 33 filters are in the output layer. The head of YOLOv3 is used as the head in YOLOv4, and the backbone is Cross Stage Partial DenseNet (CSPDarknet53). The neck is made up of Spatial Pyramid Pooling (SPP) and Path Aggregation Network (PAN). For optimization, mini-batch gradient descent with momentum is employed. Deep features from the input photos are extracted by CSPDarknet-53. SPP effectively increases the receptive field, PAN retrieves features at various scales, and the heads identify objects [25-27]. For the last layer, a linear activation function is employed. While SPP enables the network to use a variety of image sizes as opposed to the fixed-size input

image required by the conventional approach, PAN is a feature pyramid network used in YOLOv4 to increase information for segmentation [28, 29].

Upon detection of a high-touch surface, the robot by employing the use of an ultrasonic sensor computes its distance from any object or obstacle along its path. A 3-wheel robot chassis at the base of the robot, and an L298N motor driver acting as the H-bridge allows the motor rotate both clockwise and anti-clockwise. The Raspberry Pi is connected to the ultrasonic sensor and the motor driver which in turn is connected to the motors. The Raspberry Pi reads data about the surrounding of the robot using the ultrasonic sensor and sends commands to the motor driver based on this. If an obstacle is detected within a 15cm range, the Raspberry Pi instructs the motor to avoid the obstacle.

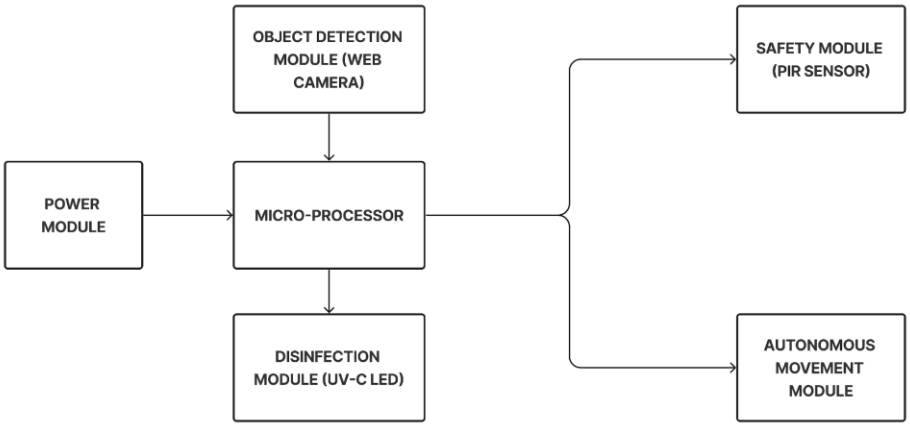

Figure 2. Block diagram of the modular classification of the UV Disinfection Robot

For UV disinfection, the system employs UVC LEDs operating at a wavelength of 275 nm as its ultraviolet light source. With a forward voltage of 5 V and a rated current of 0.1 A, 8 UVC LEDs were connected in parallel to form an LED array which was controlled by a driver circuit consisting of a relay. The UVC LED was attached to the robotic structure hosted a few centimeters above the ground. This module also included an aluminum foil reflective shield that increases the overall output and reflects UV light, boosting the effectiveness of disinfection. As shown in Figure 3, the system uses a PIR sensor with a detection range of 5 m to 12 m to identify human presence and then convey a warning in order to reduce the risks associated with exposure to UV light. When a human is detected, the Raspberry Pi turns off its UV LEDs and sounds a buzzer as a warning until it no longer detects humans.

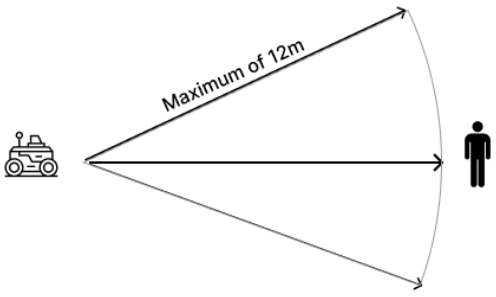

Figure 3. Human detection radius of the UV-C robot

The robot was battery-operated while the Raspberry Pi was powered by a 5 V 2.1 A power bank. A 7.4 V, 2400 mAh lithium-ion battery supplied power to the remaining circuitry. The robot's operational flowchart is shown in Figure 4. The robot moves for three seconds after starting up in an effort to find objects that are prone to contamination. The robot activates a buzzer for 0.5 seconds every 3 seconds after detecting a human until the human is no longer seen. The robot navigated to avoid an impediment that was 15 cm away and kept traveling after detecting it. When a contamination-prone object is successfully identified, the robot advances toward it, stops 20 cm away, and then moves on after disinfecting it

for 30 minutes. If the robot does not detect any contamination-prone object in 2 minutes, the robot powers off and stops its operation.

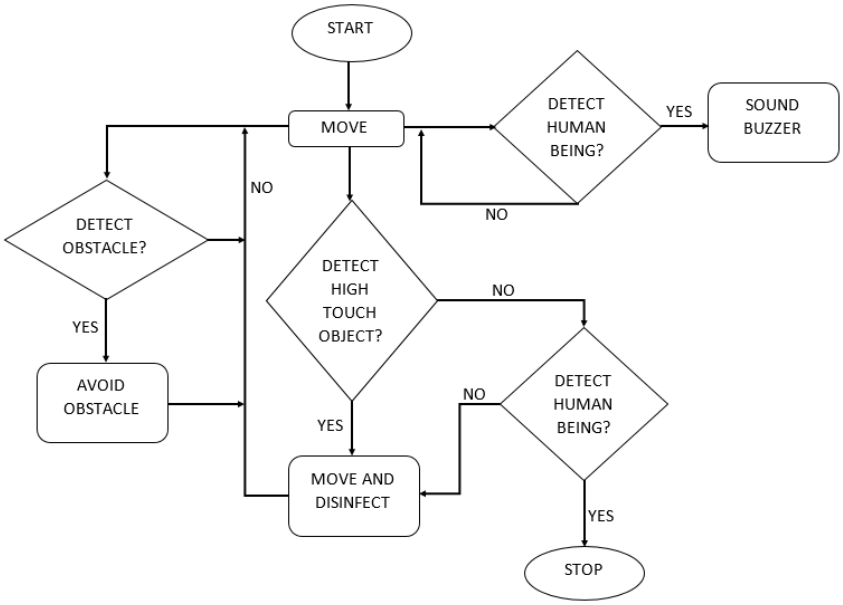

Figure 4. Flow chart of the operation of the UV Disinfection Robot

The schematic diagram of the circuit designed with Fritzing is shown in Figure 5. A voltage divider is connected to the echo pin of the ultrasonic sensor to reduce the voltage level of the echo pin from 5 V to 3.3 V. This is to protect the Raspberry Pi because the GPIO pins have an operating voltage of 3.3 V and can only read voltages up to that level [30]. Two 220 ohms resistors were connected in parallel to form a 110 ohms resistance, which was connected to the positive terminal of the UV LED array - 8 UV LEDs connected in parallel. Since connecting LEDs directly to the power supply causes them to heat up and eventually burn out, this prevents overheating and burnout of the LEDs. Through a 5 VDC relay utilized for electrical switching, the LEDs were connected to the power supply, the 5 V terminal of the L298N motor driver. By sending commands to the relays' IN pin, the raspberry pi may control the UV LEDs and subsequently the disinfection module.

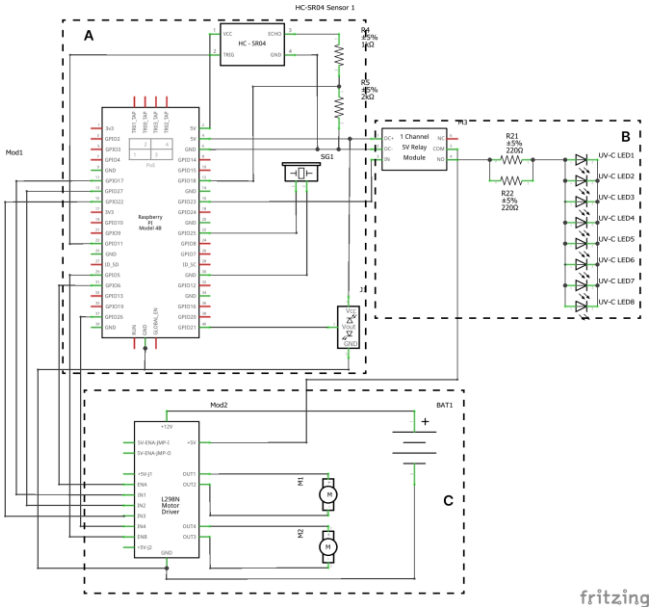

Figure 5. Complete Circuit Schematic of the UV Disinfection Robot

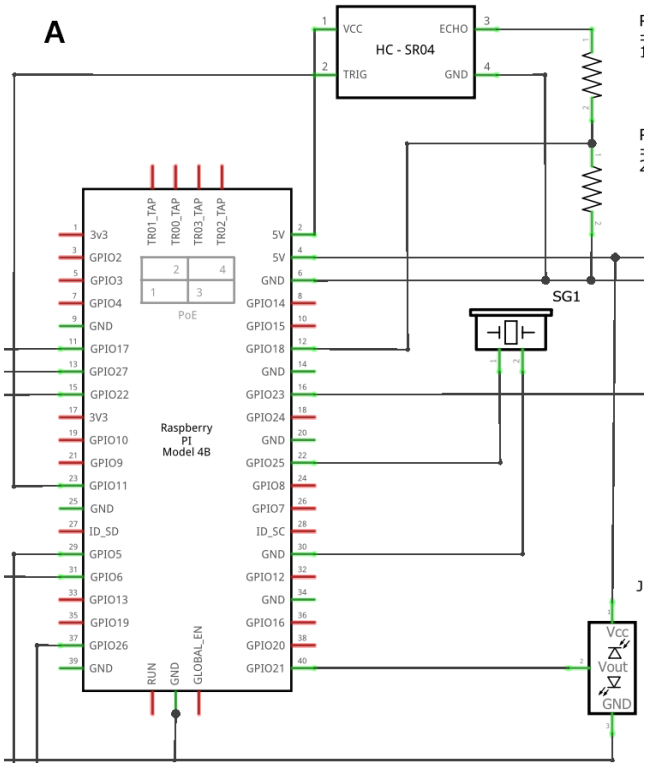

Figure 6. Section A of the UV Robot Schematic

Figure 6 shows the schematic diagram for section A of the UV robot's schematic. In this section, the ultrasonic sensor, HC-SR04 was connected to the pins of the Raspberry Pi. The VCC was connected to the 5V output of the Pi, while the echo pin was connected to GPIO 18 through a voltage divider. The trigger pin connects to GPIO 11 whereas the GND pin connects to the GND of the microprocessor. The buzzer, SG1, also had its positive and negative terminals connected to GPIO 25 and GND respectively. The PIR sensor, located at the bottom right of the image had its VCC and GND terminals connected to the 5 V and GND terminals of the Pi respectively while its Vout terminal was connected to GPIO 21.

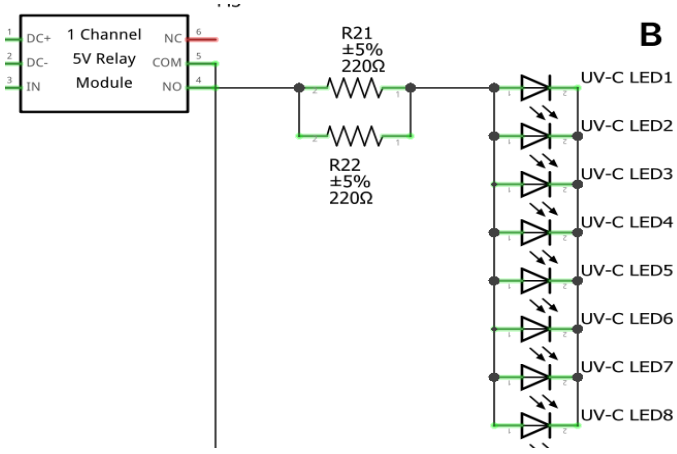

Figure 7. Section B of the UV Robot Schematic

Figure 7 shows the schematic diagram for section B of the UV robot's schematic. This section mainly functions as the UV disinfection module because it contains the UV LED arrangement and its driver circuit. The UV LED array was created by connecting two parallel 220 ohm resistors in series with an arrangement of UV LEDs that were linked in parallel. This LED array was connected to the normally-open terminal of the relay module, while the common terminal of the relay module was connected to the 5V output of the L298N motor driver. The Raspberry Pi supplied power to the relay via its

DC+ and DC- pins, and the Raspberry Pi's GPIO23 was linked to the IN pin, which was used to regulate the relay's switching.

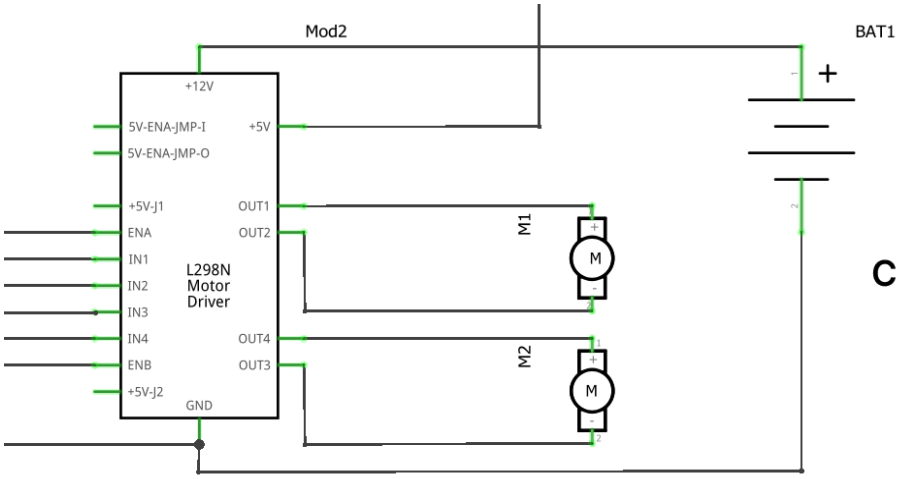

Figure 8. Section C of the UV Robot Schematic

Figure 8 illustrates the schematic diagram for section C of the UV robot's schematic. The primary function of this section is the mobility of the UV robot as both the motor driver and DC motors are connected here. OUT 1 & 2 were connected to motor M1, and OUT 3 & 4 were connected to motor M2. The motor driver was powered through its 12 V pin by the battery, BAT1. The motor was controlled through the IN and Enable pins. Pins IN 1 & 2 were used to control the motor M1 while pins IN 3 & 4 were used to control the motor M2. The enable pins, EN A & B were used to control the speed of the motors M1 and M2 respectively. These control pins were all connected to the Raspberry Pi GPIO pins and the full connection is as shown in Figure 5.

The presence of UVC light and the intensity of the radiation was measured with the aid of a UVC test dosimeter card, shown in Figure 9. The UV dosimeter card visually indicates the light energy or dosage level by 6 different gradient colors with different dosages 25 mJ/cm², 50 mJ/cm², 75 mJ/cm², 100 mJ/cm², 200 mJ/cm², 300 mJ/cm², as shown in Table 2.

Figure 9. UVC Test Dosimeter Card

Table 2 shows the available UV dosage ranges that are detectable by the UV dosimeter card and the colors for each range.

Table 2. UV Dosimeter Ranges

UV Dosimeter Range (mJ/cm^2)	Color
0 - 25	Faint purple
25 - 50	Light purple
50 - 75	Medium purple
75 - 100	Dark purple
100 - 200	Darker purple
200 - 300	Darkest purple

3. Results

The UV LED has two UVA (395–405 nm) and UVC (270–280 nm) LED chips, which together offer a twofold sterilizing effect. The primary purpose of the UVC light, at 275 nm, was to deactivate bacteria, while the primary purpose of the UVA light, at 395nm, was to serve as an indicator. Since UVC is in the invisible range of light, UVA light with a wavelength of 395 nm is used as an indication light to make sure the UVC LED is on. The color change on the dosimeter card shows the UV dosage. To evaluate the effectiveness of the UV disinfection, non-reusable UVC dosimeter cards were used to measure the UV dosage. Positioned 20 cm away from the surface to be disinfected, the dosimeter cards were exposed to UV irradiation for different durations. Figure 10 shows the readings on the UVC dosimeter test cards for the different exposure times.

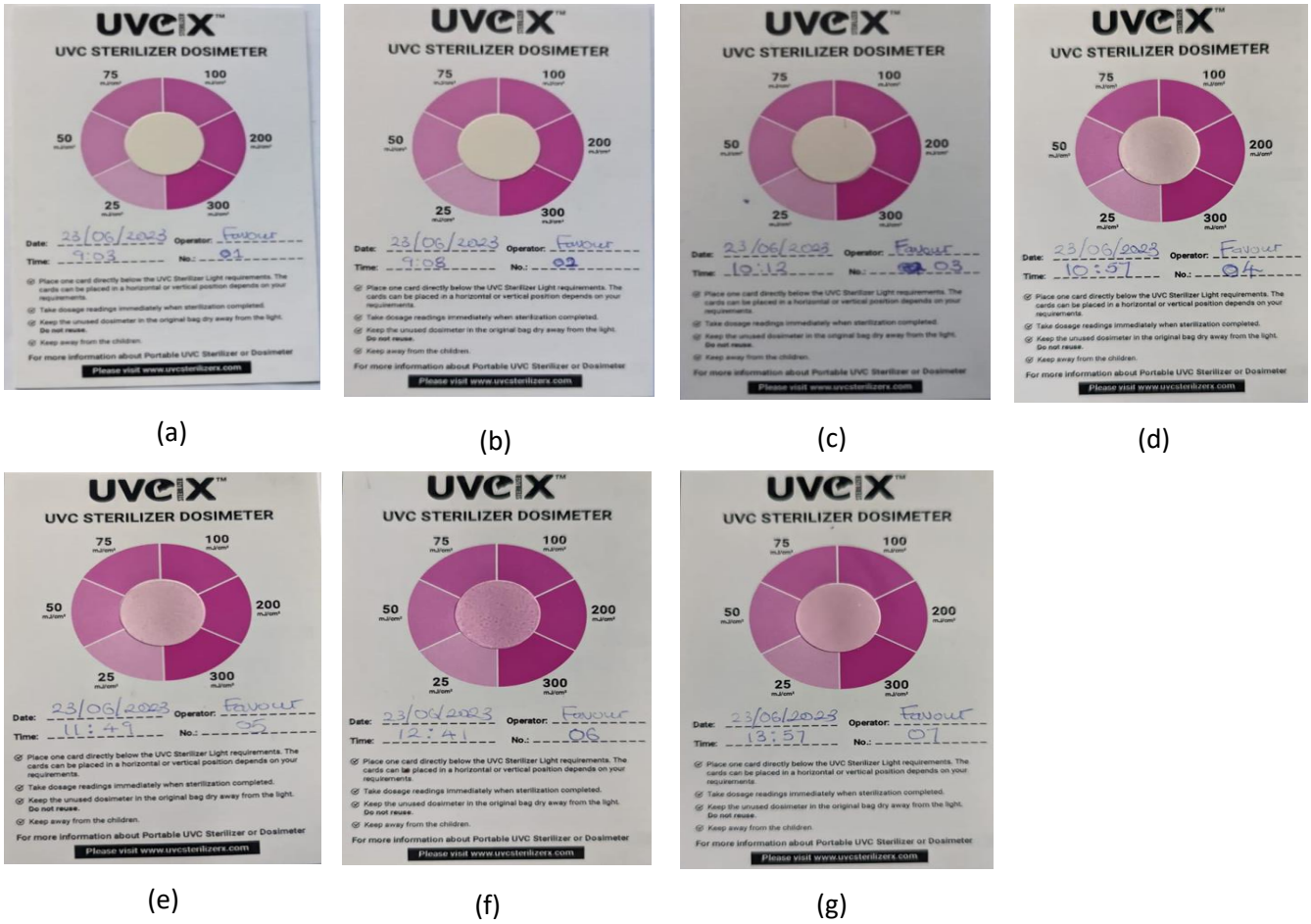

Figure 10. UV Dosimeter reading after (a) 1 minute of exposure (b) 5 minutes of exposure (c) 10 minutes of exposure (d) 20 minutes of exposure (e) 30 minutes of exposure (f) 45 minutes of exposure (g) 60 minutes of exposure

Figure 10 (a) demonstrates that the UV dosimeter card's color remained unchanged after 1 minute of exposure, making it impossible to record a reading. The UV dosimeter card's color was unchanged after 5 minutes of exposure, as shown in Figure 10 (b), and no reading could be taken. Figure 10 (c) demonstrates that the UV dosimeter card exhibits a very faint purple tint within the 0–25mJ/cm^2 range after 10 minutes of exposure. Figure 10 (d) shows that after 20 minutes of exposure, the UV dosimeter card showed a very faint purple color, which fell within the 0-25mJ/cm^2 range. Figure 10 (e) depicts that after 30 minutes of exposure, the UV dosimeter card revealed a very faint purple color, which was within the 0-25mJ/cm^2 range. Figure 10 (f) demonstrates that after 45 minutes of exposure, the UV dosimeter card showed a light purple color, which was within the 25-50mJ/cm^2 range. Figure 10 (g) also revealed that after 60 minutes of exposure, the UV dosimeter card showed a light purple color, which fell within the 25-50mJ/cm^2 range. Upon exposure to UVC light, the circular center of the dosimeter reacted to the irradiation with a color changes, depending on the UV dosage over the duration of exposure. The perimeter of the circular center was surrounded by different shades of purple representing the different ranges of the UV dosage. Upon examination of the circular center on each of the exposed dosimeter cards, the nearest color to the purple shade was recorded as the dosimeter reading for the given exposure time. The UV dosage readings taken from the UV dosimeter cards are shown in Table 3.

Table 3. UV Dosage readings over time

Exposure Time	UV Dosimeter Range	Color
1 minute	-	No detectable change
5 minutes	-	No detectable change
10 minutes	0 - 25	Very faint purple
20 minutes	0 - 25	Very faint purple
30 minutes	0 - 25	Faint purple
45 minutes	25 - 50	Light purple
60 minutes	25 - 50	Light purple

Figure 11 shows a graph of the exposure time against the UV dosimeter readings, which is the graphical representation of the UV dosages shown in Table 3.

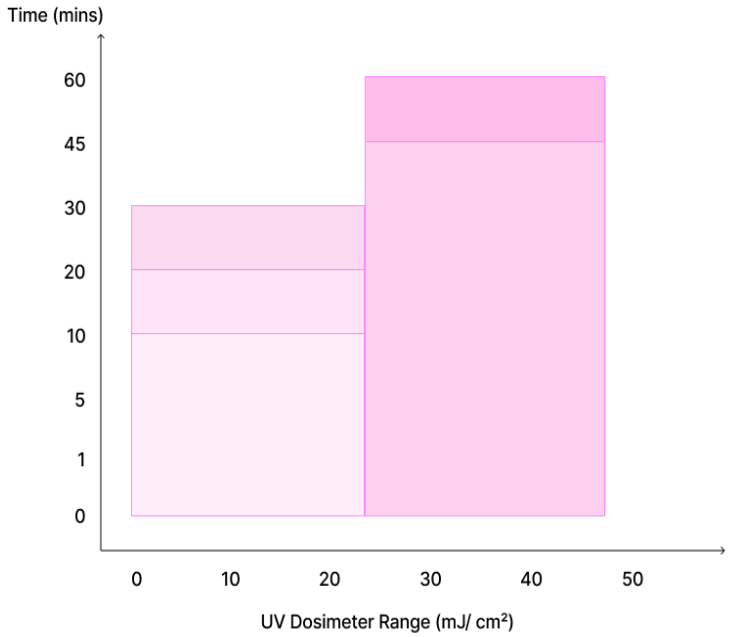

Figure 11. Graph of Time versus UV Dosimeter Readings

Figure 11 illustrates a bar chart that shows the relationship between exposure time and the UV dosimeter readings. The chart illustrates that at 1 and 5 minutes, the dosimeter displays no observable changes and is considered to read a value of zero. The UV dosimeter range is on the x-axis and the exposure period is on the y-axis. The dosimeter displayed a very

light purple tint at 10, 20, and 30 minutes that falls between 0 and 25 mJ/cm^2. The dosimeter displays a bright purple tint between 45 and 60 minutes that is between 25 and 50 mJ/cm^2. These findings demonstrate that a minimum disinfection duration of 10 minutes is necessary to perform any sort of disinfection, even if various bacteria require varied exposure times for their deactivation. Different microbes require different UVC energy levels for their effective deactivation, and Table 4 shows some microbes and their respective deactivation dosages.

Table 4. UV Dosage Required to Eliminate Microorganisms

Microbe	**Type**	**Dosage (mJ/cm^2)**
Acinetobacter baumannii	Bacteria	1.8
Bacillus megatherium	Bacteria	27.3
Listeria monocytogenes	Bacteria	15.6
Newcastle Disease Virus	Virus	1.6
Poliovirus	Virus	4.4
Adenovirus type 2	Virus	40

Data sourced from: [31].

Tables 3 and 4 show that the UV disinfection robot can successfully get rid of harmful germs while also decontaminating the contaminated surfaces. With the aid of the webcam camera and object detection model, the UV disinfection robot had the ability to detect high-touch surfaces such as door handles, and disinfect them with UV light within the germicidal wavelength. Figure 12 shows different views of the robot prototype. The UV robot avoids obstacles along its path and navigates on its own with the aid of the ultrasonic sensor. The robot shields areas outside of its line of disinfection with an aluminum shield, enabling simultaneous human cleaning, so that after disinfection, cleaning professionals can remove dust and grime. This is important to reduce cleaning time as UV disinfection only destroys microorganisms and does not clean dirt. Objects and surfaces still need to be "cleaned" to get rid of visible dirt, albeit neutralized.

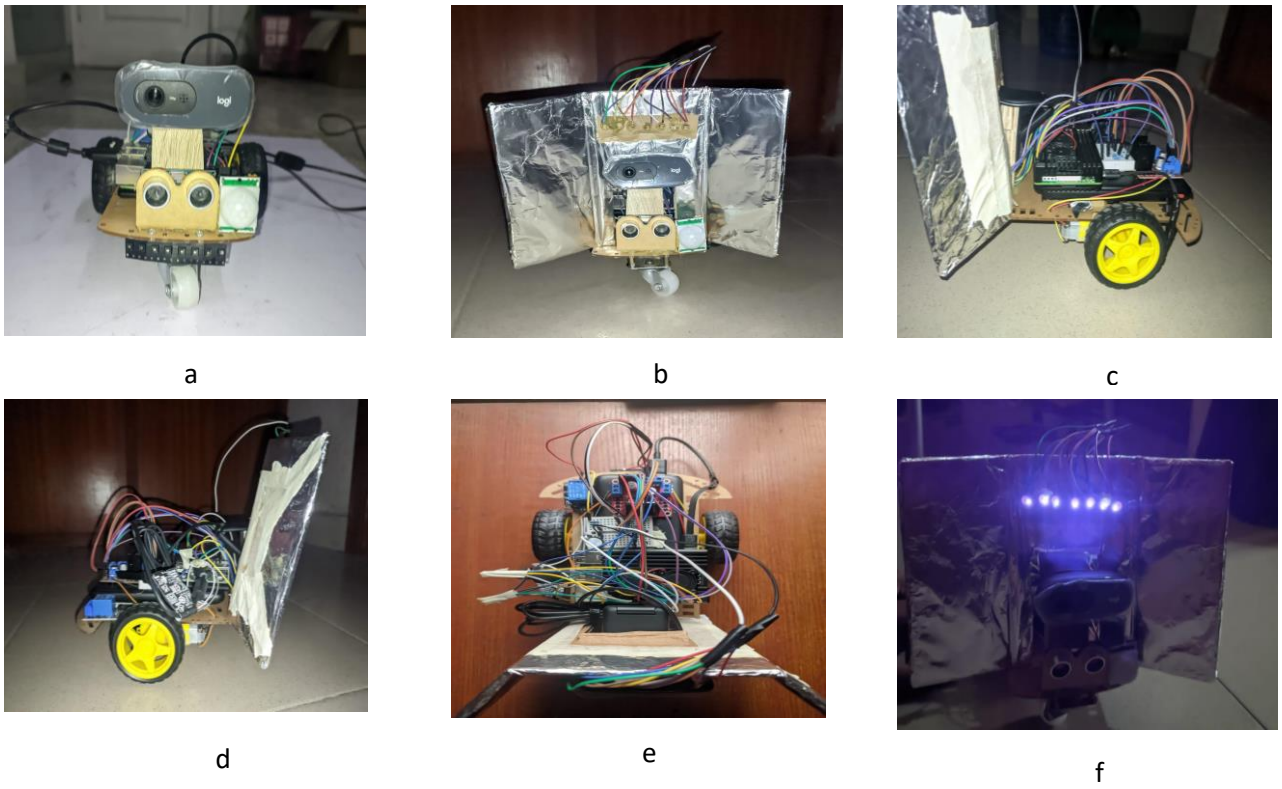

Figure 12. (a) Front view of the robot without the Aluminum shield (b) Front view of the robot with the Aluminum shield (c) Left view of the robot (d) Right view of the robot (e) Top view of the robot (f) Robot prototype with the UVC LEDs turned ON

Figure 12 (a) captures the front view of the 3-wheeled robot without the aluminum shield in view. A wooden cuboid that was affixed to the robot's chassis can be seen supporting the web camera. Along with the PIR sensor, which is placed exactly next to the web camera, the ultrasonic sensor, which is in front of it, was also glued to the robot's chassis. Figure 12 (b) captures the front view of the robot, showing the placement of the aluminum shield on the robot chassis, as well as the location of the UVC LED arrangement. The aluminum shield is affixed to the bottom of the robot chassis and is constructed from cartons covered in aluminum foil. The breadboard, which is connected by the wires that are visible coming out of the LED setup, is shown in other figures. Figure 12 (c) shows the left view of the robot with the Raspberry Pi, power bank, breadboard, motor driver, left DC motor, and wheel in view. The Raspberry Pi, breadboard, and motor driver were all adhered to the top of the power bank, which was bonded to the robot's chassis. The arrangement aimed to maximize the limited space available, while also ensuring that all necessary ports to the Pi remained accessible. The jumper wires used for the connection between the components and the breadboard are shown. Figure 12 (d) shows the left view of the robot with the power bank, relay, motor driver, right DC motor, and wheel in view. The relay was used to control the switching of the UVC LED array and can be seen to be glued to the robot chassis. The cable connecting the web camera to the USB port of the Pi and some other ports on the Pi are equally shown. Figure 12 (e) shows the top view of the UV robot prototype with the majority of the interconnected components in view. As the jumper wires coming out of the Raspberry Pi are linked to the breadboard, relay, and motor driver, it is visible inside the aluminum shell that houses it. It can be seen that the power cable is attached to the power bank that powers the Raspberry Pi. On the breadboard, the jumper wires from the UV LED array in front of the robot are connected in series with a parallel arrangement of two 220 ohm resistors, and the relay is connected after that. On the robot chassis, the left and right wheels are where the jumper cables are shown coming from. Figure 12 (f) shows the UV robot with the LED array powered ON. It should be noted that the reflection angle of this prototype takes a range from 20^o to 25^o on both sides respectively. The Aluminum shield reflects the UV light and prevents it from reaching behind the device. This allows further human activities behind the robot and out of risk. The autonomous UV disinfection robot is a significant achievement in the field of robotics engineering and disinfection technology. It effectively combines obstacle avoidance, UV disinfection, and object detection to create a solution for contamination-prone environments. The use of an Aluminum shield ensures targeted disinfection and increases efficiency while allowing for human activities away from the line of disinfection. A key innovation of this study is the integration of object detection with real-time disinfection, which optimizes the process and makes it environmentally friendly. This robot is particularly relevant in high-risk environments such as hospitals and shared spaces, and its autonomous nature minimizes the need for human interference, reducing potential exposure to pathogens and improving hygiene standards. This robot opens the door to numerous applications in industrial facilities, hospital settings, and public venues.

4. Conclusion

This article has presented an effective and efficient approach for surface disinfection by implementing UVGI with the aid of UVC LEDs and a robot for autonomous navigation. It prioritizes the autonomy of the disinfection robot due to the advantages it has over fixed UV-C systems. The efficiency of the robot's functioning was boosted by the employment of integrated sensors and cameras. The capacity of the robot to function safely in the presence of humans was a key consideration during the design process. Although UV-C effectively inhibits microorganisms, it does not get rid of dust and dirt that may be present on surfaces. Due to this, its applicability in spaces that are not completely vacant was also taken into consideration. The robot allows for simultaneous human cleaning, by shielding the areas that are out of its line of disinfection with an aluminum foil so that cleaning staff could get rid of dust and dirt after disinfection has occurred. This effectively reduces the total sanitization time and optimizes the processes involved. The UV robot could be adopted in places like hospitals or medical centers where sick people are often located. Some of the possible innovations in the future work will be to explore the possibility of improving upon the efficiency of the UV disinfection robot. UV light source at a wavelength of 254 nm could be investigated as well. To improve the accuracy of the autonomous navigation, a more accurate technique such as Lidar sensor or camera-based techniques could be investigated. Since objects beyond the maximum height of the robot are not disinfected because they are beyond the reach of the robot, further research may be carried out in designing a robot that could adjust the height of the UV light sources relative to object detection using AI. The robot may also experience trouble navigating in tight spaces due to its form factor and as such, certain corners and shadow areas may not be captured. The surfaces and surface shapes where microbes and viruses are found could be investigated in future work as well.

5. Author Contribution Statement

In this study, Author 1 contributed to forming the idea, design, manuscript preparation, and critical review; Author 2 contributed to the design and manuscript preparation.

6. Ethics Committee Approval and Statement of Conflict of Interest

"There is no need for an ethics committee approval in the prepared article"
"There is no conflict of interest with any person/institution in the prepared article"

7. List of Abbreviations

AI	Artificial Intelligence
COVID – 19	Coronavirus Disease 2019
CSPD	Cross Stage Partial DenseNet
GND	Ground
GPIO	General Purpose Input/Output
LED	Light Emitting Diode
LMP	Low Pressure Mercury
PAN	Path Aggregation Network
PIR	Passive Infrared
SPP	Partial Pyramid Pooling
UV	Ultraviolet
UVGI	Ultraviolet Germicidal Irradiation
YOLO	You Only Look Once

8. References

[1] Guettari M, Gharbi I, Hamza S. "UVC disinfection robot". *Environmental Science and Pollution Research*, 28, 40394–40399, 2021.
[2] Sanchez AG, Smart WD. "Verifiable Surface Disinfection Using Ultraviolet Light with a Mobile Manipulation Robot". *Technologies*, 10, 48, 2022.
[3] McGinn C, Scott R, Ryan C, Donnelly N, Cullinan MF, Beckett M. "Rapid disinfection of radiology treatment rooms using an autonomous ultraviolet germicidal irradiation robot". *American Journal of Infection Control*, 50(8), 947-953, 2022.
[4] Schahawi MD, Zingg W, Vos M, Humphreys H, Lopez-Cerero L, Fueszi A, Zahar JR, Presterl E. "Ultraviolet disinfectioonrobots to improve hospital cleaning: Real promise or just a gimmick? *Antimicrobial Resistance & Infection Control*, 10, 33, 2021.
[5] de Zoysa H, Morecroft E. "Cleaning, disinfection and sterilization of equipment". *Anaesthesia & Intensive Care Medicine*, 8(11), 453–456, 2007.
[6] Mehta I, Hsueh H, Taghipour S, Li W, Saeedi S. "UV disinfection robots: a review". *Robotics and Autonomous Systems*, 161, 104332, 2023.
[7] Dancer SJ. "Controlling hospital-acquired infection: Focus on the role of the environment and new technologies for decontamination". *Clinical Microbiology Reviews*, 27(4), 665 - 690, 2014.
[8] Vyshnavi A., Manasa AN, Hamsika SS, Shalini P. "UV Disinfection robot with automatic switching on human detection". *EAI Endorsed Transactions on Internet of Things*, 6(23), 1-6, 2020.
[9] UVO3. "The History of Water Treatment". https://www.uvo3.co.uk/the-history-of-uv-disinfection-uvo3/ (18.12.2022).
[10] HEPACART. "Far-UV VS. Near-UV". https://www.hepacart.com/blog/far-uv-vs.-near-uv (31.05.2017).
[11] World Health Organization, "Radiation: Ultraviolet (UV) radiation". https://www.who.int/news-room/questions-and-answers/item/radiation-ultraviolet (uv)#:~:text=The%20UV%20region%20covers%20the,(100%2D280%20nm) (26.09.2023).
[12] Brandt K.S. "Why UV light is one of the most effective ways to sanitize your home". https://www.insider.com/does-uv-light-kill-germs (18.12.2022).
[13] Mehta I, Hsueh HY, Taghipour S, Li W, Saeedi S. "UV disinfection robots: A Review". *Robotics and Autonomous Systems*, 161, 104332, 2023.
[14] Ackerman E. "Autonomous robots are helping kill coronavirus in Hospitals". IEEE Spectrum. https://spectrum.ieee.org/autonomous-robots-are-helping-kill-coronavirus-in-hospitals (08.01.2023).
[15] Anderson, M. "UV light might keep the world safe from the coronavirus-and whatever comes next". IEEE Spectrum. https://spectrum.ieee.org/uv-light-might-keep-the-world-safe-from-the-coronavirusand-whatever-comes-next (09.01.2023).
[16] Building Momentum. "UV-C robot 2.0: After a design sprint and the completion of a first prototype, building momentum's UV-C robot is stronger and more powerful than ever". https://web.facebook.com/watch/?v=636986286901250 (08.01.2023).
[17] Shen Y. Guo D, Long F, Mateos LA, Ding H, Xiu Z, Hellman RB, King A, Chen S, Zhang C, Tan H. "Robots under covid-19 pandemic: A comprehensive survey". *IEEE Access*, 9, 1590–1615, 2021.
[18] McGinn C, Scott R, Donnelly N, Roberts KL, Bogue M, Kiernan C, Beckett M. "Exploring the applicability of robot-assisted UV disinfection in Radiology". *Frontiers in Robotics and* AI, 7, 1-12, 2021.
[19] Ackerman E. "Akara Robotics turns Turtlebot into autonomous UV disinfecting robot". IEEE Spectrum. https://spectrum.ieee.org/akara-robotics-turtlebot-autonomous-uv-disinfecting-robot (27.04.2020).
[20] Simmons SE, Carrion R, Alfson KJ, Staples HM, Jinadatha C, Jarvis WR, Sampathkumar P, Chemaly RF, Khawaja F, Povroz-nik M, Jackson S, Kaye KS, Rodriguez RM, Stibich MA. "Deactivation of SARS-COV-2 with pulsed-xenon ultraviolet light: Implications for environmental covid-19 control". *Infection Control & Hospital Epidemiology*, 42(2), 127–130, 2020.
[21] Hyun KS. "KIST's Efforts to Overcome COVID-19". Korean Institute of Science and Technology. https://www.kist.re.kr/_attach/kist/old/9/2021112511482543_0.pdf (08.01.2023).
[22] Moore SK "Flight of the GERMFALCON: How a potential coronavirus-killing airplane sterilizer was born". IEEE Spectrum. IEEE Spectrum. https://spectrum.ieee.org/germfalcon-coronavirus-airplane-ultraviolet-sterilizer-news (Accessed: 08.01.2023).

[23] Chanprakon P, Sae-Oung T, Treebupachatsakul T, Hannanta-Anan P, Piyawattanametha W. "An ultra-violet sterilization robot for disinfection". Proceeding - 5th International Conference on Engineering, Applied Sciences and Technology, 2019.
[24] Perminov S, Mikhailovskiy N, Sedunin A, Okunevich I, Kalinov I, Kurenkov M, Tsetserukou D. "UltraBot: Autonomous Mobile Robot for Indoor UVC Disinfection". IEEE 17th International Conference on Automation Science and Engineering (CASE), 2147-2152, 2021.
[25] Bochkovskiy A, Wang C, Liao HM. "YOLOv4: Optimal speed and accuracy of object detection". *ArXiv*, *abs/2004*.10934, 1-17, 2020.
[26] Li Y, Wang H, Dang LM, Nguyen TN, Han D, Lee A, Jang I, Moon H. "A deep learning-based hybrid framework for object detection and recognition in autonomous driving". *IEEE Access*, 8, 194228–194239, 2020.
[27] Liu H, Fan K, Ouyang Q, Li N. "Real-time small drones detection based on pruned yolov4". *Sensors*, 21(10), 3374, 2021.
[28] He K, Zhang X, Ren S, Sun J. "Spatial pyramid pooling in deep convolutional networks for visual recognition". IEEE transactions on pattern analysis and machine intelligence, 37(9), 1904–1916, 2015.
[29] Liu S, Qi L, Qin H, Shi J, Jia J. "Path aggregation network for instance segmentation". IEEE conference on computer vision and pattern recognition, 8759–8768, 2018.
[30] Pounder L. "Raspberry Pi Gpio Pinout: What each pin does on PI 4, earlier models, Tom's Hardware". https://www.tomshardware.com/reviews/raspberry-pi-gpio-pinout,6122.html#:~:text=The%20operating%20voltage%20of%20the,(see%20resistor%20color%20codes) (12.04.2023).
[31] UV Light Technology. "UVC dose required to kill microorganisms". Available at: https://uv-light.co.uk/uv-dosage-required-to-kill-microorganisms/ (24.06.2023).